Università degli Studi di Padova

Dipartimento di Beni Culturali: Archeologia, Storia dell'Arte, del Cinema e della Musica

Corso di Laurea Magistrale in
SCIENZE ARCHEOLOGICHE
Curriculum in
APPLIED SCIENCES TO CULTURAL HERITAGE,
MATERIALS AND SITES

Archaeometric study of mortars from the Roman Villa of Mutteron dei Frati, Bibione, Italy

Supervisor:
Prof. Michele Secco
Co-supervisors:

Prof. Simone Dilaria
Prof. Maria Stella Busana
Dr. Valeria Razzante

Candidate:
Ekaterina Sokolova
Reg. number 2070767

Academic year 2023/2024

List of contents

List of figures

List of tables

Acknowledgments

I would like to express my sincere gratitude to everyone who contributed to the completion of this master's thesis.

First and foremost, I am deeply thankful to my thesis advisors, Michele Secco and Simone Dilaria, for their invaluable guidance, patience, and encouragement throughout this research journey. Their expertise and insightful feedback were crucial in shaping this thesis.

Special thanks go to my co-advisors Maria Stella Busana and Valeria Razzante, for providing the necessary resources and facilities that allowed me to collect the necessary data.

Heartfelt thanks to my family and friends for their unwavering support, understanding, and encouragement throughout this academic journey.

Lastly, I would like to acknowledge the individuals whose work and contributions were cited in this thesis, as well as all those who, in various ways, contributed to this research effort.

Thank you all for your support and belief in my abilities.

Ringraziamenti

Vorrei esprimere la mia sincera gratitudine a tutti coloro che hanno contribuito alla realizzazione di questa tesi di laurea magistrale.

Prima di tutto, sono profondamente grato ai miei relatori di tesi, Michele Secco e Simone Dilaria, per la loro guida inestimabile, pazienza e incoraggiamento durante questo percorso di ricerca. La loro competenza e i loro preziosi suggerimenti sono stati cruciali per dare forma a questa tesi.

Un ringraziamento speciale va alle mie correlatrici Maria Stella Busana e Valeria Razzante, per aver fornito le risorse e le strutture necessarie che mi hanno permesso di raccogliere i dati necessari.

Un sentito grazie alla mia famiglia e ai miei amici per il loro costante supporto, comprensione e incoraggiamento durante questo percorso accademico.

Infine, vorrei ringraziare le persone i cui lavori e contributi sono stati citati in questa tesi, così come tutti coloro che, in vari modi, hanno contribuito a questo sforzo di ricerca.

Grazie a tutti per il vostro sostegno e per aver creduto nelle mie capacità.

Abstract

The archaeological site at Bibione di San Michele al Tagliamento, Italy, has been the focus of excavations and reconnaissance efforts since the discovery of its initial artifacts in 1760. Significant excavations were carried out by Bertolini in 1903 and Cassi in 1932, providing preliminary insights into the site's historical context. Further exploration was undertaken by the Superintendency of Padua in 1991. The site exhibits evidence of two distinct construction phases: the first phase, dating from the end of the 1st century BC to the 1st century AD, is characterized by meticulously constructed limestone walls with gray cement and substantial foundations. The second phase, dating to the 4th-5th century AD, features less precisely built walls composed of limestone fragments and brick mulch.

In August 1991 and 1994, the Archaeological Superintendency for the Veneto conducted targeted excavations near the sandy relief known as "Mutteron dei Frati" in Bibione di San Michele al Tagliamento. These efforts focused on classical period coastal settlements, uncovering a significant Roman maritime villa. This villa exhibited two distinct sectors: an older eastern sector characterized by narrow, elongated rooms and perimeter walls, and a later western sector constructed with reused materials.

Subsequent excavation campaigns since 2022 have uncovered additional parts of the buildings, offering new insights into the site's historical and architectural features. Samples collected during the 2022, 2023, and 2024 excavation campaigns are currently under study, contributing to a deeper understanding of the site's significance within the context of Roman-era coastal settlements.

This dissertation undertakes an archaeometric evaluation of wall mortars from the Roman Villa of Mutteron dei Frati, Bibione. The analysis of mortar samples follows a methodological approach progressing from general to specific, employing techniques such as colorimetry, X-ray powder diffraction (XRPD), petrographic analysis using optical microscopy (OM), and scanning electron microscopy (SEM). Alongside the analysis, a comprehensive literature review was conducted to establish the chronological framework and significance of the studied constructions and the city itself. This contextual understanding enhances the interpretation of the analytical results within the unique historical and archaeological contexts of the site.

The primary objective of this study is to elucidate the composition, manufacturing methods, and chemical processes involved in mortar production, thereby contributing to a deeper understanding of ancient construction practices and materials.

Sommario

Il sito archeologico di Bibione di San Michele al Tagliamento, in Italia, è stato oggetto di scavi e ricerche sin dalla scoperta dei suoi primi reperti nel 1760. Scavi significativi furono condotti da Bertolini nel 1903 e da Cassi nel 1932, offrendo primi approfondimenti sul contesto storico del sito. Ulteriori esplorazioni furono intraprese dalla Soprintendenza di Padova nel 1991. Il sito mostra evidenze di due distinti fasi di costruzione: la prima fase, che risale dalla fine del I secolo a.C. al I secolo d.C., è caratterizzata da mura di calcare costruite con cura, cemento grigio e fondazioni consistenti. La seconda fase, risalente al IV-V secolo d.C., presenta mura costruite con meno precisione, composte da frammenti di calcare e malta di mattoni.

Nell'agosto del 1991 e nel 1994, la Soprintendenza Archeologica per il Veneto ha condotto scavi mirati nei pressi dell'area sabbiosa conosciuta come "Mutteron dei Frati" a Bibione di San Michele al Tagliamento. Questi sforzi si concentrarono sugli insediamenti costieri del periodo classico, portando alla luce una significativa villa marittima romana. Questa villa presentava due settori distinti: un settore orientale più antico caratterizzato da stanze strette e allungate e mura perimetrali, e un settore occidentale più recente costruito con materiali riutilizzati.

Le campagne di scavo successive dal 2022 hanno portato alla luce parti aggiuntive degli edifici, offrendo nuove intuizioni sulle caratteristiche storiche e architettoniche del sito. Campioni raccolti durante le campagne di scavo del 2022, 2023 e 2024 sono attualmente oggetto di studio, contribuendo a una comprensione più profonda del significato del sito all'interno del contesto degli insediamenti costieri dell'epoca romana.

Questa dissertazione si propone di condurre una valutazione archeometrica delle malte delle pareti in muratura della Villa Romana di Mutteron dei Frati a Bibione. L'analisi dei campioni di malta segue un approccio metodologico che va dal generale allo specifico, utilizzando tecniche come la colorimetria, la diffrazione ai raggi X delle polveri (XRPD), l'analisi petrografica tramite microscopia ottica (OM) e la microscopia elettronica a scansione (SEM). In aggiunta alle analisi archeometriche, è stata condotta una revisione esaustiva della letteratura per stabilire il quadro cronologico e il significato delle costruzioni studiate e della città stessa. Questa comprensione contestuale migliora l'interpretazione dei risultati analitici all'interno dei contesti storici e archeologici unici del sito.

L'obiettivo principale di questo studio è quello di chiarire la composizione, i metodi di produzione e i processi chimici coinvolti nella produzione delle malte, contribuendo così a una comprensione più profonda delle pratiche e dei materiali edilizi dell'antichità.

Chapter 1. Introduction

The territories of the former Roman empire inherited a big number of material culture objects which still captivate the interest of scientists and scholars all over the world. Architectural structures and archaeological sites are one of the most important compounds of this legacy. Ancient Roman wall mortars offer invaluable insights into the construction techniques and material technologies of one of history's most influential civilizations, as they directly impact on the durability and stability of the buildings. The Roman villa of Mutteron dei Frati serves as a remarkable case study for understanding these techniques. By examining the mortars used in this villa, we can uncover details about the materials and methods employed by Roman builders in the present-day region of Veneto, Northern Italy.

As part of the project framework, this study aims to conduct an archaeometric analysis of the wall mortars used in the Roman villa of Mutteron dei Frati. Mortar samples were collected from this site during various excavation campaigns. These samples were subsequently analyzed using techniques such as colorimetry, X-ray powder diffraction (XRPD), optical microscopy, digital image analysis, and scanning electron microscopy coupled with energy dispersive spectroscopy (SEM-EDS). The observations and analyses of these mortar samples aim to enhance the understanding of their composition, quality, and manufacturing techniques.

1.1 Objectives

The main objective of this study is to perform an archaeometric analysis of the mortars used in the villa of Mutteron dei Frati. This involves examining mortar samples from various parts of the villa using a range of analytical techniques. The research will systematically investigate the physical properties, mineralogical profiles, and chemical composition of the collected mortar samples. Through this comprehensive analysis, the study aims to gain a detailed understanding of the composition, manufacturing techniques, and chemical processes involved in the production of these mortars.

1.2 Research plan

- Conduct a literature review of mortar composition, properties, manufacturing procedures, and the applicable analytical techniques.
- Reconstruct the historical and geographical context of the construction of the Roman villa through a bibliographic review.
- Utilize and implement various analytical techniques to observe the general composition of the wall mortars.
- Identify the chemical and mineralogical compositions of the wall mortar samples.
- Define the various construction phases and techniques applied to the building process of the villa.

Chapter 2. Mortars

Mortar is a workable paste constituted by a mixture of sand, a binder, and water, which hardens to bind masonry units, to fill and seal the irregular gaps between them, spread the weight of them evenly, and sometimes to add decorative colors or patterns to masonry walls.

Mortars, as cultural artifacts, exhibit characteristics and properties shaped by the raw materials employed and the technological expertise of their creators. They are integral in imparting strength, protection, and aesthetic qualities to structures. The study of ancient mortars holds dual significance: firstly, it provides valuable insights into the raw materials and technologies accessible during their creation, and secondly, it is crucial for understanding their primary physical properties and current state of preservation, which is essential for restoration and conservation efforts. Earth science methodologies are applicable in assessing the primary characteristics and properties of ancient mortars and their components, including both binders and aggregates. Due to the impracticality of directly measuring all properties of the binders and aggregate fractions, some properties must be inferred through data processing [1].

2.1 Mortars properties and characteristics

Lime, which was first manufactured as early as 12,000 BCE, is created by burning limestone ($CaCO_3$), with the formation of quicklime (CaO) through the so-called calcination process. The decomposition temperature of limestone can vary depending on its composition and the ambient pressure during burning. However, to thoroughly calcine limestone, the raw material needs to be maintained at a constant temperature of 750–850°C for several hours. For producing large quantities of quicklime, temperatures of 800–900°C must be sustained for three to four days [2]. Excessive temperatures are avoided because they produce unreactive "dead-burned" lime. The quality of the binder is influenced by various factors, such as the composition, porosity, and impurity content of the fired limestone, as well as the maximum temperature and the time-temperature path of the firing process, and the conditions of slaking. The initial limestone should have a non-carbonate mineral content (typically silicates and clays) of less than 5-10 wt%, and the carbonate should consist of pure calcium. The fired blocks are ground into a fine powdered quicklime, which is unstable under normal humidity conditions and tends to hydrate into portlandite (calcium hydroxide, $Ca(OH)_2$). If the CaO powder is mixed with an exact (stoichiometric) amount of water (lime/water = 75.7/24.3 = 3.12 by weight), the result is a fine dry powder, and the process is known as dry hydration because there is just enough water to produce portlandite. When the CaO powder is mixed with excess water, it forms a smooth paste or slurry, a process referred to as lime slaking. The portlandite paste (slaked lime or lime putty) can then be used as a binder and for architectural purposes (such as filler, adhesive, crack sealer, floor consolidant, and surface smoother) or as a raw material for modeling objects, vessels, and even artwork.

The process by which limestone (calcium carbonate) is converted to quicklime by heating, then to slaked lime by hydration, and naturally reverted to calcium carbonate by carbonation is called the lime cycle [3]. This process is illustrated in Figure 1.

LIMESTONE
Calcium carbonate
($CaCO_3$)

calcined
(roasted)
(heat added)

Calcium hydroxide reverts
back to Calcium carbonate,
releasing water
$Ca(OH)_2 + CO_2 = CaCO_3 + H_2O$

The
Lime
Cycle

hardening
Slaked lime
absorbs CO_2
from the air

QUICKLIME
Calcium Oxide
($CaO + CO_2$)

SLAKED LIME
Calcium hydroxide
$CaO + H_2O = Ca(OH)_2$

Slaking
(water added)
$CaO + H_2O$
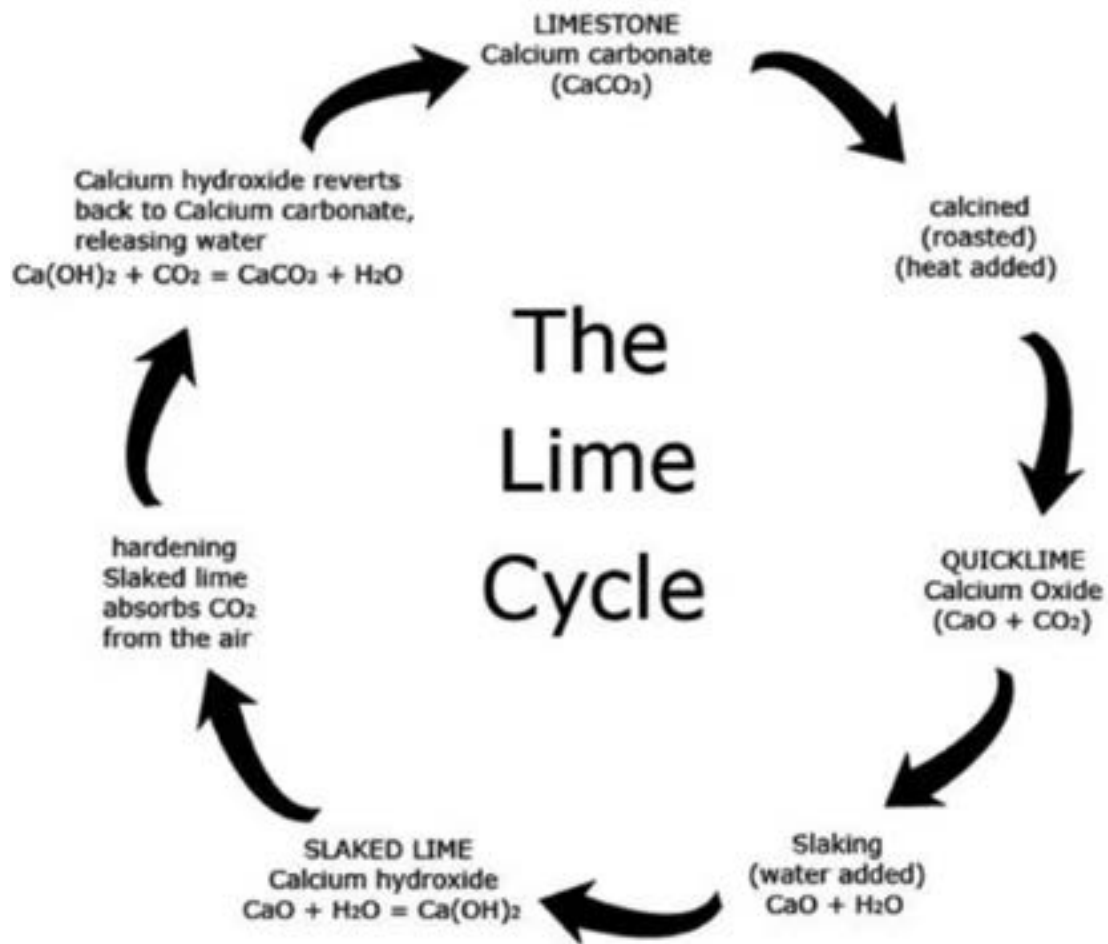
Fig. 1 – The lime cycle (Source: Marlborough Chalk: Reflections on the College, its history and its area)

Chapter 3. Historical context of San Michele al Tagliamento, Bibione

The name "Bibione" appears in chronicles and imperial certificates from the 9th century, referring to an island between Grado and Caorle, though its exact location is now lost. Ancient chronicles, such as Chronicon Altinate (8th century) and records by Diacono Giovanni, Costantino Porfirogenito, Ottone I, and Bernardo di Cerclaria, describe the area near the coast. However, Venetian historians have debated the name and location due to the lack of archaeological and archival evidence. The coastal area now known as Baseleghe, mentioned in early chronicles as Bibione, was a significant harbor during Roman and Byzantine times, located at the outlet of the "Tiliaventum Maius" river. Later, a community with a church and refreshment place was documented there. In the 13th century, trade immunities granted by Venice extended from Baseleghe to Primero. By the 14th century, Baseleghe became a preferred trading route due to canal excavations. It remained a trading hub among Venice, Caorle, Grado, and Aquileia, and included a "palada", a "postarollo", and a small military post with a protective pine forest [4].

The first discoveries in the area were made in 1760, followed by systematic excavations by Bertolini in 1903 and Cassi in 1932 at the "Mutteron dei Frati" site [5]. In August 1991 and 1994, the Archaeological Superintendency for the Veneto conducted two excavation tests at the "Mutteron dei Frati" site, located within the agricultural company "Val Grande" in Bibione di San Michele al Tagliamento. These investigations aimed to analyze the typological and architectural characteristics of classical period coastal settlements near the mouths of the Canal dei Lovi and the Tagliamento River [6].

One of the first written sources about the villa describes the area as the pine forest in a scenic peninsula in the Portogruaro district, rich in natural beauty and owned by Mr. Caccia of Trieste. During enhancement work, ancient Roman construction remains were discovered, including walls and intricate mosaics. The excavation revealed various artifacts, including coins (copper coin of Julian, one of Flavius Victor, two other coins from the later periods), nails, glass fragments, and pottery. The findings suggest the presence of a noble Roman villa, contrasting with a previously believed medieval castle. The discovery highlights the historical significance and the transformation of structures over centuries in the area [7].

The research, carried out by Andrea Battiston and Vincenzo Gobbo in the end of the 20th century, identified two construction phases of the villa (Fig.2).
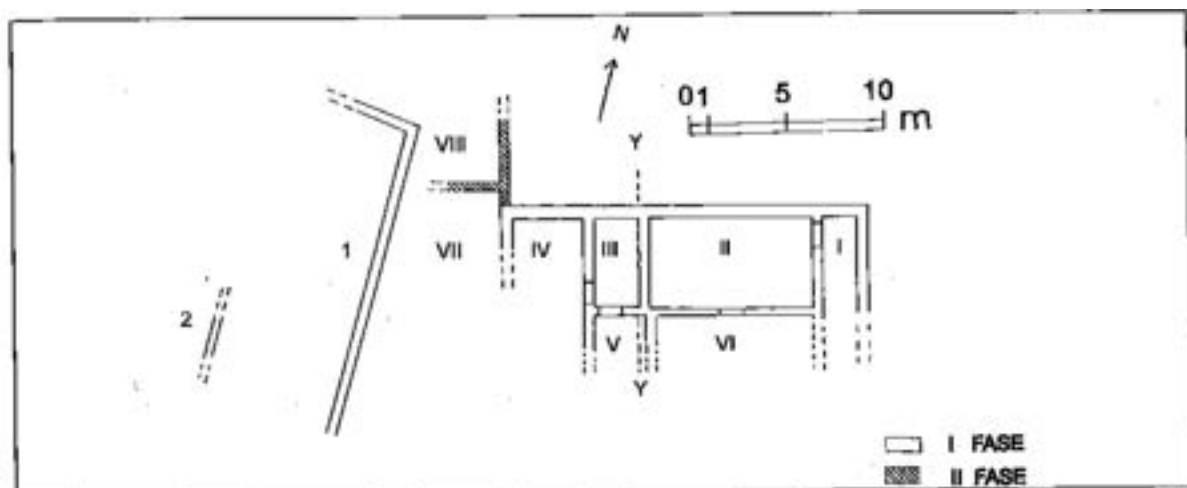
Fig. 2 – Planimetry of the villa (credits: Busana 2002))

Phase I

The original Roman building consisted of rooms I to VI. Excavations revealed the northern sector, identifying the perimeter walls to the north, west, and east, covering about 130 square meters (18.5 x 7 meters). These structures, oriented 18°-19° NW, extended southward, with the eastern area likely occupied by a courtyard.

The layout was an elongated rectangle, oriented east-west (parallel to the coastline), with contiguous rooms arranged in sequence, forming one or two rows. The rooms opened southward towards the shoreline.

13

The uncovered sector served a residential purpose: except for Room V, which lacked a preserved floor, all other rooms had mosaic floors. Rooms III (4.30 x 2.25 m) and IV (partial 6 x 3.60 m) had white tesserae floors bordered by black tesserae strips, likely used as bedrooms or dining rooms. Rooms II (8.25 x 4.30 m) and VI (8.25 x 1.30 m partial) were large adjoining rooms with an east-west orientation, Room VI having a floor similar to Room III. Room I (7.60 x 1.80 m partial) had a white mosaic floor, serving as a corridor connecting Room II to the eastern courtyard.

The masonry structures, including thresholds, were made of limestone blocks from Carso, bound with strong mortar. The northern perimeter wall (0.60 m thick) had an internal ledge and 1-meter-deep foundations, built against the ground and supported by pre-Roman sandy dunes.

Additional masonry structures to the west, likely part of a second structure oriented approximately north-south, included a section of the eastern perimeter wall (E) ending in a room with a mosaic floor and the northeast corner of the parallel perimeter wall (2), 6.50 meters from the main building. The two complexes were separated by 5-10 meters

Phase II

In the late 4th century AD, the building expanded westward, possibly connecting with a western settlement, creating trapezoidal spaces. The southern area (VII) was paved with *cocciopesto*, while the northern area (VIII) remained unpaved.

This phase featured masonry structures made of stone blocks with brick fragments. The northern extension of the northern perimeter wall maintained 1-meter-deep foundations, using a construction technique against the ground.

The Phase I building dates to the end of the 1st century BC to early 1st century AD, as indicated by mosaics in rooms III-V and other materials. The building expanded in the late 4th century AD, as evidenced by a coin of Honorius found in the foundations of Room VIII.

The settlement was likely located along the lagoon route between Ravenna and Aquileia, between the mouths of the Tiliaventum Maius and Tiliaventum Minus rivers.

Aerial photography identified two road routes: one from the Mutteron dei Frati settlement towards the inlet of Porto Baseleghe, following the ancient coastline and revealing sporadic Roman materials; the other from the northern edge of Valle Grande heading north, passing between two Roman settlements [8].

Since 2022 the research restarts under the guidance of professor Dirk Steuernagel, supported by dr. Alice Vacilotto and Lorenzo Cigaina (University of Regensburg), in collaboration with professor Maria Stella Busana (University of Padua), confirming the presence of multiple phases and providing many new data about the plan of the villa.

3.1 Geological context of San Michele al Tagliamento, Bibione

Bibione, located in the municipality of S. Michele al Tagliamento in the northern province of Venice, is a peninsula bordered by the Tagliamento River, the Adriatic Sea, Porto Baseleghe, and the Litoranea Veneta canal. It connects to the mainland via a single bridge and has an area of 28.41 square kilometers, featuring a 10.4 km coastline, valleys, and pine forests. The territory on which Bibione is situated, and more generally the entire Venetian Plain, was formed through the transport and deposition of materials eroded from upstream areas during numerous alluvial cycles. The geology of the area is thus characterized by multiple layers of material with varying grain sizes (clays, silts, and sands) that overlap and intersect, creating a diverse and complex structure. [9]

Holocene deltaic systems along the Mediterranean coast exhibit geomorphological features influenced by factors such as sea-level changes, alluviation, geological structure, and human activities. Initially, natural factors were predominant, but human influence has grown significantly over the past 6000 years, particularly in the last 2000 years. Research on the interaction between human societies and their environment in deltaic plains has intensified in recent decades, focusing on flood risk management in wetland areas.

Geoarchaeological data indicate that ancient waterways in the Aquileia plain, primarily to the east, were more significant than current rivers. Core deposits reveal at least two historical rivers, with an older north-south course and later northeast-southwest direction, likely due to natural or artificial causes such as eustatism and neotectonics. These rivers transported gravel deposits absent in the south and west of Aquileia, creating uncertainty in tracing their paths to the sea and identifying ancient river mouths (Fig.3) [10]. This information is crucial for understanding the geological context of Bibione as the distance between two sites is around 46.5km which makes them similar in terms of geomorphological processes.
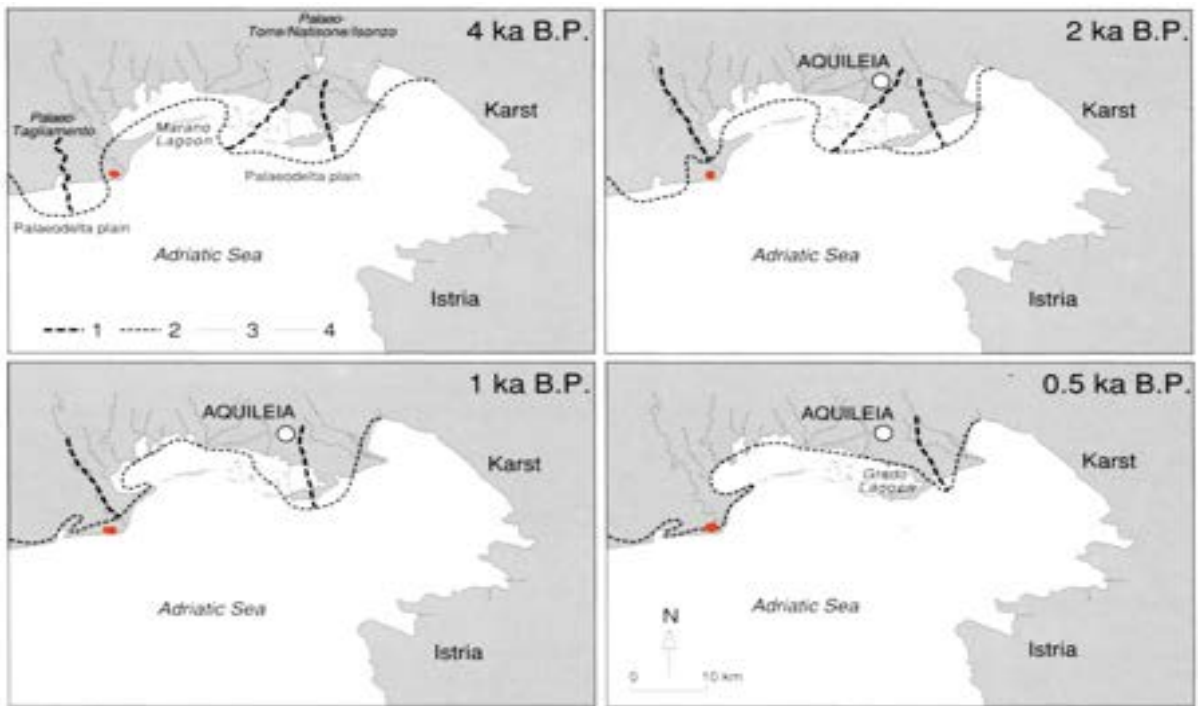
Fig. 3 – Palaeogeography of the Aquileia deltaic plain at various time intervals (modified after Marocco, 1991). 1: distributary palaeochannel, 2: palaeocoastline, 3: present river, 4: present coastline. Bibione is marked as a red dot in all the four images
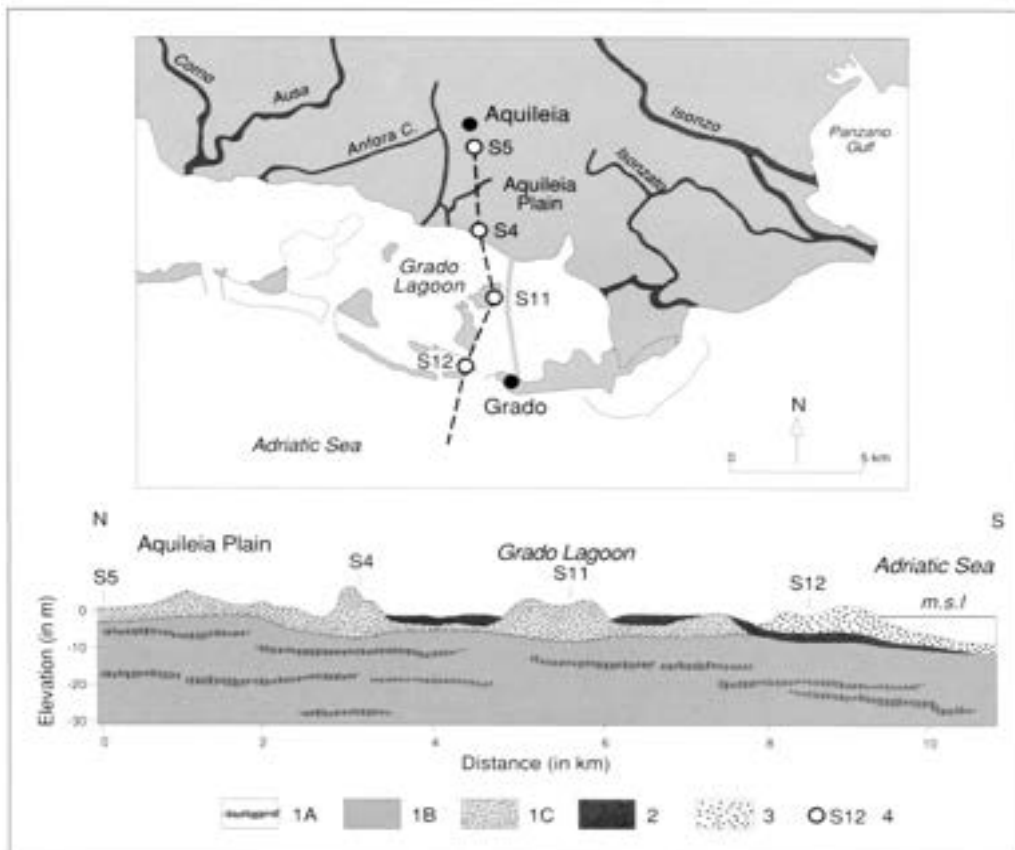
Fig. 4 – Depositional palaeoenvironments in the Aquileia deltaic plain (modified after Marocco et al., 1984). 1: continental deposits (1A = peat; 1B = silt; 1C = sand); 2: lagoonal deposits; 3: marine deposits; 4: borehole.

In the same study, Arnaud and Fassetta discussed the sedimentation present in the same area. Fig.4 shows depositional palaeoenvironments in the Aquileia deltaic plain.

Another study carried out by Gazzi in 1973 [11] investigated the compositional features of sands from present beaches and rivers, analyzing 71 samples collected between the Isonzo and Foglia mouths in the northern Adriatic. The data revealed regional patterns that identify and characterize seven major sedimentary petrological provinces, define their boundaries, and determine the influence of various rivers on sand supply and littoral dispersal.

Isonzo River sands are distributed as far as Lignano. These sands have high carbonate grain contents, with calcite slightly exceeding dolomite, and feature a heavy mineral assemblage with picotite and ultrastable minerals such as zircon, tourmaline, and rutile.

From the Tagliamento River to the Po delta, dolomite content exceeds calcite, and carbonate grains decrease southward.

This information is also valuable for understanding the sediment composition of Bibione, given its proximity to the locations studied by Gazzi.

The current position of the Tagliamento River's mouth and delta was established around 18,000 years ago, following the melting of the Alpine glaciers. During the last glaciation, lower sea levels (130 meters below current levels) turned the upper Adriatic Sea into a flat, muddy plain. The Po, Adige, Piave, and Tagliamento rivers combined to form a large delta near Pescara. Rising sea levels eventually submerged this delta, leading to the rivers becoming independent and each forming its own delta. The Tagliamento's delta is shaped by the sea's wave motion and coastal currents, redistributing sands along the coast. Wind further shapes the sandy coast, forming and stabilizing dunes, which protect against storm surges. These dunes act as sand reservoirs, preventing coastal erosion. However, if dunes are destroyed for development, coastal erosion can occur as the sea takes away the beach sands [12].

Chapter 4. Sampled Areas

52 samples of various materials from different areas of the villa were taken (Fig.5a,b). They comprise 11 samples of wall-paintings, 13 of preparatory layers for floors and 28 of wall mortars. The complete list of samples and their brief description is reported in table 1 and their amount in the dataset is graphically represented in table 2. Figure 6 reports the general plan of the villa where sampling points were highlighted. In order to simplify the readability of the map, different colors and abbreviations were assigned to different types of samples. The abbreviation BB stands for the name of the site (Bibione). Wall mortar samples are named WM and a sequential number and have a red color, wall-painting samples are named INT and a sequential number and have a magenta color, whereas the preparatory samples for floors are named PREP and a sequential number and have a green color.

<div align="center">Fig.5a   Fig.5b</div>

Fig. 5 – The sampling process. a) excavation campaign 2023, b) excavation campaign 2024

Table 1. Full list of samples taken from the Villa Mutteron dei Frati during the excavation campaigns 2022-2024

Sample	Strat.unit	Chronology	Description	Structure
BB_INT_01A		Roman age	Rinzaffo	raised, perimeter S; stone wall made of roughly squared limestone ashlars arranged with the more regular side towards the outside of the structure to create a double facing; the space between the two is filled with stone chips and brick fragments, also used in the vestments to fill the gaps; sub-horizontal courses

Sample	Strat.unit	Chronology	Description	Structure
BB_INT_01B		Roman age	Arriccio+ intonachino	raised, perimeter S; stone wall made of roughly squared limestone ashlars arranged with the more regular side towards the outside of the structure to create a double facing; the space between the two is filled with stone chips and brick fragments, also used in the vestments to fill the gaps; sub-horizontal courses
BB_INT_02A		Roman age	Rinzaffo	elevation, wall between room F and H; wall in similar technique to the S perimeter wall; plastered on the W front
BB_INT_02B		Roman age	Arriccio	elevation, wall between room F and H; wall in similar technique to the S perimeter wall; plastered on the W front
BB_INT_02C		Roman age	Intonachino	elevation, wall between room F and H; wall in similar technique to the S perimeter wall; plastered on the W front
BB_INT_03	USM3	Roman age	Intonaco	USM3, raised; N-S stone wall
BB_INT_04_A	US104	Roman age	Plaster, first layer	
BB_INT_04_B	US104	Roman age	Plaster, second layer	
BB_INT_05_C	USM101	Roman age	Plaster, third layer	
BB_INT_05_D	USM101	Roman age	Plaster, fourth layer	
BB_INT_05_E	USM101	Roman age	Plaster, paint layer	

Sample	Strat.unit	Chronology	Description	Structure
BB_INT_09	US215	Roman age		
BB_INT_10	US401	Roman age		
BB_PREP_01	US14	Roman age	Base concrete of the floor	room G, brick floor; beaten sample US1002 = 5
BB_PREP_02	US1002	Roman age	Cocciopesto floor	room G, brick floor; beaten sample US1005 = 14
BB_PREP_03	US8	Roman age	Upper floor preparation	US8
BB_PREP_04	US12	Roman age	Upper floor preparation	US11 pavement
BB_PREP_05	US28	Roman age	Base concrete of the floor	US28 pavement
BB_PREP_06	US156	Roman age	Base concrete of the floor	
BB_PREP_07	US124	Roman age	Cocciopesto floor	
BB_PREP_08	US157	Roman age	Base concrete of the floor	
BB_PREP_08_S	US157	Roman age	Calcination relict inside BB_PREP_08	
BB_PREP_09	US124	Roman age	Cocciopesto floor	
BB_PREP_10	US143	Roman age	Base concrete of the floor	
BB_PREP_11	US126	Roman age	Upper floor preparation	
BB_PREP_12	US125	Roman age	Mortar layer of the mosaic tesserae	
BB_PREP_13	US413	Roman age	Mosaic preparational mortar	mosaics preparation mortar
BB_PREP_14	US411	Roman age	Mosaic preparational mortar	
BB_PREP_15	US403	Roman age		
BB_PREP_16	US216	Roman age		

Sample	Strat.unit	Chronology	Description	Structure
BB_PREP_17	US307	Roman age	Upper layer of the pavement	coarse cocciopesto
BB_PREP_18	US313	Roman age	Earthern mortar pavement	
BB_PREP_19		Roman age		Pavement under 313, visible in section
BB_WM_01		Roman age	Bedding mortar	raised, perimeter S; stone wall made of roughly squared limestone ashlars arranged with the more regular side towards the outside of the structure to create a double facing; the space between the two is filled with stone chips and brick fragments, also used in the vestments to fill the gaps; sub-horizontal courses
BB_WM_02		Roman age	Bedding mortar	elevation, wall between room F and H; wall in similar technique to the S perimeter wall; plastered on the W front
BB_WM_03		Roman age	Bedding mortar	raised, perimeter E room F; terracing wall against the dune; similar technique to the other structures
BB_WM_04		Roman age	Bedding mortar	elevation, wall between rooms F and C;
BB_WM_05	USM4	Roman age	Bedding mortar	USM4, raised; E-W stone wall, core and facing. Binds to USM3; at the external corner you can see a squared stone block
BB_WM_06	USM3	Roman age	Bedding mortar	USM3, raised; N-S stone wall
BB_WM_07	USM2	Roman age	Bedding mortar (upper level)	USM2; E-W stone wall, in the N facing some reused

Sample	Strat.unit	Chronology	Description	Structure
				tiles and pebbles can be recognized
BB_WM_08	USM2	Roman age	Bedding mortar (lower level)	USM2; E-W stone wall, in the N facing some reused tiles and pebbles can be recognized
BB_WM_09	USM5	Roman age	Bedding mortar	USM 5
BB_WM_10	US18	Roman age	Bedding mortar	USM1; E-W wall; very deep limestone foundations; irregularly shaped ashlars arranged in sub-horizontal courses
BB_WM_11	USM6	Roman age	Bedding mortar	USM6; first phase wall with NW-SE orientation; same technique
BB_WM_12		Roman age	Bedding mortar	elevation N-S, perimeter E room C
BB_WM_13		Roman age	Bedding mortar	elevation E-W, perimeter N room C
BB_WM_14	US116	Roman age	Lean concrete over the foundation of the wall	
BB_WM_15	USM102	Roman age	Foundation mortar	
BB_WM_16	US132	Roman age	Lean concrete over the foundation of the wall	
BB_WM_17	USM102	Roman age	Mortar at the base of the wall	
BB_WM_17_B	USM102	Roman age	Recycled plaster inside BB_WM_17	
BB_WM_18	USM101	Roman age	Foundation mortar	
BB_WM_19	USM101	Roman age	Mortar at the base of the wall	

Sample	Strat.unit	Chronology	Description	Structure
BB_WM_20	USM101	Roman age	Foundation mortar	
BB_WM_21	USM104	Roman age	Foundation mortar	
BB_WM_22	US400	Roman age	Bedding mortar	
BB_WM_23	US201	Roman age	Bedding mortar	
BB_WM_24	US200	Roman age	Bedding mortar	
BB_WM_25	US202	Roman age	Bedding mortar	
BB_WM_26	US317	Roman age	Bedding mortar	
BB_WM_27	USM300	Roman age	Bedding mortar	

Table 2. Graphical representation of the proportion of collected samples.
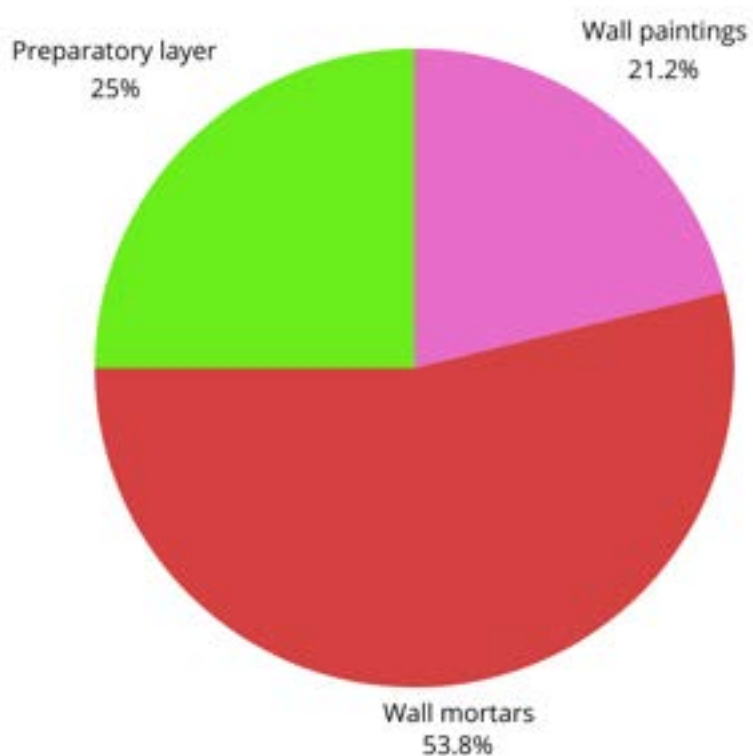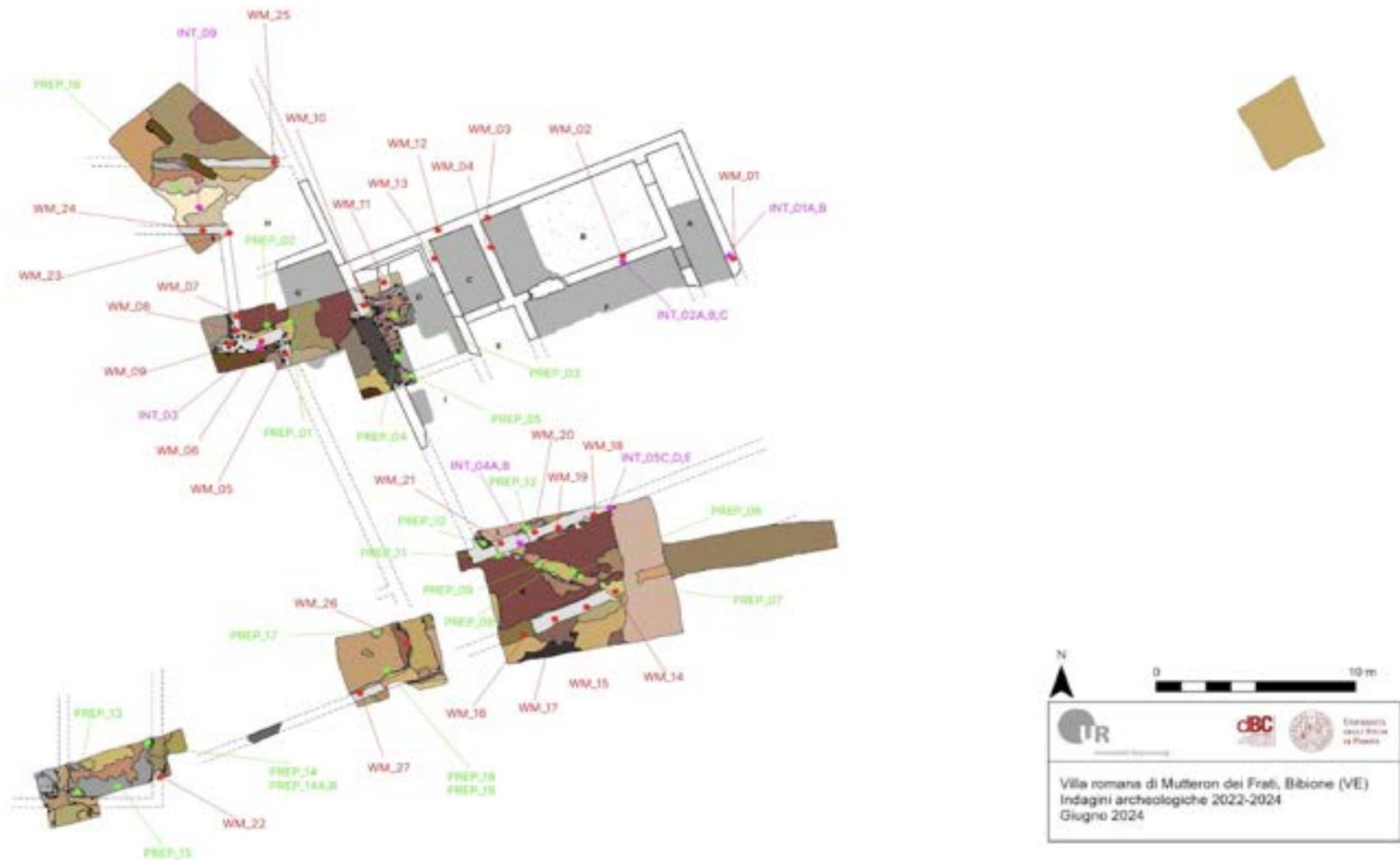
Fig. 6 – Mortar sampling points from the excavation campaigns 2022-2024The samples were taken by manual removal by using chisels and hammers during the excavation seasons 2022, 2023 and 2024. The analyses of the samples were carried out in the laboratories of the Department of Geosciences of the University of Padova.

Chapter 5. Materials and methods

Most of the samples underwent the colorimetry and XRPD analysis, however, due to their big number, it was decided to focus only on the wall mortar ones for further analysis such as optical microscopy, image analysis and SEM-EDS. Table 3 represents the list of samples and the analysis they underwent.

Table 3. The list of samples and analysis

Sample	Colorimetry	XRPD	Optical microscopy	SEM-EDS	Image analysis
BB_INT_01A	X	X			
BB_INT_01B	X	X			
BB_INT_02A	X	X			
BB_INT_02B	X	X			
BB_INT_02C	X	X			
BB_INT_03	X	X			
BB_INT_04_A		X			
BB_INT_04_B		X			
BB_INT_05_C		X			
BB_INT_05_D		X			
BB_INT_05_E		X			
BB_PREP_01	X	X			
BB_PREP_02	X	X			
BB_PREP_03	X	X			
BB_PREP_04	X	X			
BB_PREP_05	X	X			
BB_PREP_06	X	X			
BB_PREP_07	X	X			

Sample	Colorimetry	XRPD	Optical microscopy	SEM-EDS	Image analysis
BB_PREP_08	X	X			
BB_PREP_08_S	X	X			
BB_PREP_09	X	X			
BB_PREP_10	X	X			
BB_PREP_11	X	X			
BB_PREP_12	X	X			
BB_WM_01	X	X	X		X
BB_WM_02	X	X	X		X
BB_WM_03	X	X	X		X
BB_WM_04	X	X	X		X
BB_WM_05	X	X	X		X
BB_WM_06	X	X	X		X
BB_WM_07	X	X	X		X
BB_WM_08	X	X	X		X
BB_WM_09	X	X	X	X	X
BB_WM_10	X	X	X		X
BB_WM_11	X	X	X	X	X
BB_WM_12	X	X	X		X
BB_WM_13	X	X	X		X
BB_WM_14	X	X	X		X
BB_WM_15	X	X			
BB_WM_16	X	X	X	X	X
BB_WM_17	X	X	X	X	X
BB_WM_17_B	X	X			

Sample	Colorimetry	XRPD	Optical microscopy	SEM-EDS	Image analysis
BB_WM_18	X	X			
BB_WM_19	X	X	X		X
BB_WM_20	X	X	X		X
BB_WM_21	X	X			
BB_WM_22	X	X	X	X	X
BB_WM_23	X	X	X		X
BB_WM_24	X	X	X		X
BB_WM_25	X	X	X		X
BB_WM_26	X	X	X		X
BB_WM_27	X	X	X	X	X

5.1 XRPD

X-ray diffraction (XRD) is a versatile, non-destructive analytical technique used to analyze material properties such as phase composition, structure, and texture in powder samples, solid samples, or even liquid samples. XRPD measurements were conducted using a PANalytical X'Pert PRO diffractometer (Fig.7) in Bragg-Brentano geometry, equipped with a cobalt X-ray tube and an X'Celerator detector. The operating conditions were as follows: CoKa radiation, 40 kV voltage, 40 mA current, 2θ range of 3-85°, step size of 0.02°, and 100 seconds counts per step. Mineral phases were identified with X'Pert HighScore Plus software, and further quantitative analysis was performed using Rietveld refinement with Topas software.

Phase identification is accomplished by comparing the X-ray diffraction pattern of an unknown sample to patterns contained within a reference database, analogous to the matching of fingerprints in forensic investigations. The most extensive database is curated by the International Centre for Diffraction Data (ICDD). Furthermore, a reference database can be constructed from experimental diffraction patterns of pure phases, as well as from patterns published in scientific literature or acquired through personal measurements [13].

Fig. 7 – Philips X'Pert PRO diffractometer, Bragg-Brentano geometry with Bragg-Brentano HD optics, cobalt source, X'Celerator detector, and Anton Paar HTK16 hot stage. (source: https://www.geoscienze.unipd.it/diffrattometria-x-polveri)

X-ray diffraction (XRD) relies on the constructive interference of monochromatic X-rays with a crystalline sample. These X-rays are generated by a cathode ray tube, filtered for monochromatic radiation, collimated, and directed at the sample. Constructive interference occurs when the conditions of Bragg's law are met [14].

Figures 8a-8j illustrate the sample preparation process for X-ray Powder Diffraction (XRPD) analysis. The sample, or a portion thereof, must first be ground (Fig. 8a). Depending on the sample's hardness, this can be accomplished using different methods. If the sample is particularly hard, initial grinding with the Retch BB50 grinding machine is recommended (Fig. 8b), followed by further grinding with a mortar and pestle (Fig. 8c). For softer samples, the grinding can commence directly with the mortar and pestle.

Subsequently, the ground sample should undergo three cycles of micronization using the RD-Mill McCrone machine (Fig. 8d). This process employs a container with zirconia cylinders (Fig. 8e), to which 15 ml of deionized water is added. The first cycle, lasting 2 minutes, serves to clean the container. During the second cycle, a spatula of the sample and an additional 15 ml of deionized water are added, with this cycle also lasting 2 minutes. The third and final cycle involves the preparation of the sample itself, where 4 spatulas of the sample and 15 ml of ethanol are placed in the container, with the cycle duration extended to 5 minutes. This

results in a liquid sample, which is then poured onto a laboratory plate and allowed to dry (Fig. 8f). The use of ethanol accelerates the drying process.

The dried sample is carefully removed from the plate using a razor and prepared for the next stage. For analysis, it is necessary to mix the sample with a standard reference material, in this case, zincite. An OHAUS PR series electronic scale is used to accurately weight the sample and the standard in the appropriate proportions (Fig. 8g). The ideal mixture consists of 80% sample powder (0.8 g) and 20% zincite (0.2 g). After weighing, these components are thoroughly homogenized using a mortar and pestle.

The final step of this preparation process involves transferring the homogenized powder mixture into a sample holder, ensuring it is evenly distributed and properly packed. Once the sample is securely in the holder, it is ready for measurement (Figs. 8i-8j).

Fig.8a

Fig.8b

Fig.8c

Fig.8d

Fig.8e

Fig.8f

Fig.8g

Fig.8h

Fig.8i

Fig.8j

Fig. 8 –Preparation of the sample for XRPD analysis (photo by Sokolova E.)

5.2 Colorimetry

Colorimetry is the science of the measurement of color, replacing subjective responses of colors with an objective numerical system. Perception of the color of an object is governed by three factors: the nature of the illumination, the optical properties of the object itself and the response of the human eye. Colorimetry quantitates these aspects and introduces the concepts of standard illumination and observers, leading to color representations such as RGB, XYZ, L*a*b* and L*C*h° to unambiguously define color [15].

Colorimetry is based on the principle that when monochromatic light passes through a colored solution, the solution's coloring substances absorb part of the light, with the remaining light being transmitted. The intensity of the color is proportional to the concentration of the analyte responsible for the color [16].

The color of mortar can provide important information about its composition, including the types of raw materials used and their sources. Variations in color can indicate differences in the mineralogical composition and the presence of additives or pigments. The colorimetric study of mortars can reveal historical construction techniques and technological advancements. Different periods and cultures may have used distinct methods and materials, which can be identified through color analysis. It also provides quantitative data that can be systematically recorded and compared.

The process of acquisition of color values for each of the 49 samples was performed with the use of the colorimeter PCE-XXM 30 of PCE-instruments with an angle measurement of D/8-SCI, an aperture of 8∅, and a range of wavelength of 400-700 nm (Fig.9). The time of acquisition per sample was of less than a minute and the color code was given on the L*a*b* color space. The color measurements were done on the powdered form of the mortar due to the homogenization it provides of both binder and aggregates. There was no need for further preparation of the samples since the powdered form of the mortars was recovered from the preparation treatments for XRPD analysis. It should be highlighted that the color acquisition was performed on the mortar powder without the addition of zinc oxide, since this could result in a variation of the true color values of the sample.

Fig. 9 – Colorimetric analysis (photo by Sokolova E.)

5.3 SEM-EDS

A large depth of field sets scanning microscopy apart from other techniques, enabling direct observation of fracture surfaces in solid mortar samples. The microscope offers a resolution of a few nanometers. Scanning electron analysis is utilized to evaluate particle shape and size, morphology, the relationships between mortar constituents, and to detect inclusions, cracks, void filling, and pore shapes. One significant advantage of this method is the relatively simple sample preparation required. In certain techniques, such as backscattered electron imaging, observations are made on polished sections. Coupling an energy-dispersive X-ray spectrometer (EDS) with a scanning electron microscope allows for rapid analysis of elemental composition. Ensuring the representativeness of the sample is crucial for interpreting the microstructure observed at such a small scale [17].

The instrument is based on an electron microscope, which generates an image of the specimen by bombarding it with a beam of electrons. Various phenomena result from the collision between electrons and the specimen's atoms, but the most relevant to this research are the scattering of the electron beam and the emission of X-rays. X-rays are emitted when atoms in the specimen absorb energy from the electron beam and become excited. These atoms can then relax and emit X-rays. A key feature of this technique is that X-ray emission is not random; different atomic elements within the specimen emit rays with characteristic energies. Thus, the X-ray emission provides information about the atoms present in the specimen, making the technique similar to XRF [18].

The 30-micron thin section requires additional polishing to be suitable for SEM-EDS analysis. This task was performed using the Struers LaboPol-35 machine (Fig. 10) in the laboratory of the Department of Geosciences at the University of Padova.

In scanning electron microscopy, conductive coatings are frequently applied to the surfaces of insulating or beam-sensitive materials, including biological specimens, polymers, ceramics, geological samples, and semiconductors. These coatings, which can be metals like gold, platinum, and iridium or non-metals such as carbon, help to dissipate charge build-up and minimize structural damage caused by the electron beam. In case of this analysis, the samples were coated with gold.

Fig. 10 – Struers LaboPol-35 polishing machine (photo by Sokolova E.)

The prepared samples were then individually analyzed using a Coxem tabletop SEM EM-30 plus (Fig.11) with an acceleration voltage of 20 kV. Observations were made at variable

magnifications using backscattered electrons to gather chemical information about the samples. Additionally, semi-quantitative elemental composition was determined through EDS analysis.
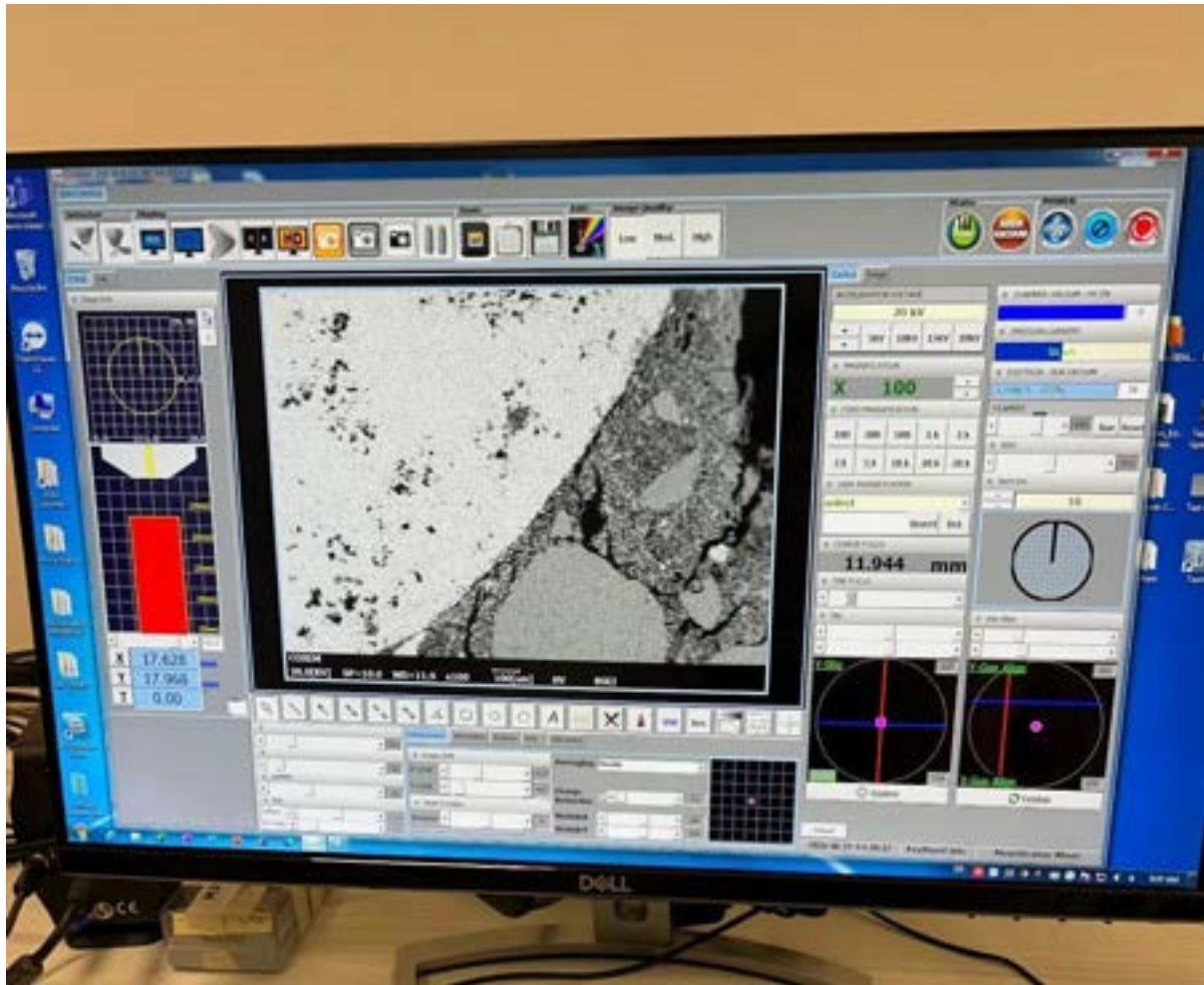
Fig. 11 COXEM software interface (photo by Sokolova E.)

After performing the SEM-EDS analysis, concentrations of the major elements Al, Fe, Si, Ca, and Mg were determined by analyzing selected areas of the binder.

Hydraulic limes contain enough free CaO to be slaked with water and can set underwater. A minimum amount of free CaO in the calcined product is necessary to reduce the entire mass to powder when slaked, as the reaction with water causes expansion and disintegration of the freshly burnt limestone. However, if there is too much free CaO, the product cannot harden underwater. Products meeting these criteria vary widely and are typically classified based on their chemical composition, specifically their cementation or hydraulicity index. Boynton (1966) proposed classifying hydraulic limes into feebly, moderately, and eminently hydraulic categories [19].

The hydraulicity of the mortar was assessed using the hydraulicity index (HI) calculated as: $HI(Al_2O_3 + Fe_2O_3 + SiO_2)/(CaO+MgO)$. The HI index is proportional to the mortar's ability to harden in wet or water-saturated environments. An HI value below 1.2 corresponds to the upper

limit for quick-setting lime. Higher HI values indicate the presence of minute silicate rock or mineral fragments in the selected area, which increases the levels of Al_2O_3, Fe_2O_3, and SiO_2 in the analysis and does not reflect the true amount of hydraulic reaction products.

5.4 Optical microscopy

Optical microscopy is a fundamental technique in the study and analysis of mortars which uses cross- and plane-polarized light. This method allows for detailed examination of the mineralogical and textural properties of mortar samples, providing insights into their composition, preparation, and condition. The minero-petrographic study of mortars allows highlighting various aspects of the binder, such as mineralogical composition, birefringence color, texture (micritic, microsparitic, sparitic), structure (homogeneous, presence of patches, etc), interactions with the aggregate (e.g. reaction edges), presence of lumps [20]. The observations were carried out on the thin sections (30 μm) of samples by means of a Leica DM750 P Polarized Light Microscopy (PLM) in transmitted light (TL) operating with the integrated digital camera FLEXACAM C1 with objectives 1.6X, 4X, and 10X. The microscope utilized for this purpose includes essential components such as an illuminator or light source, a polarizer, a condenser, a diaphragm, an aperture, a stage, objectives with varying magnifications, a compensator, an analyzer, and an eyepiece. Fig.12 illustrates the components of an optical microscope.
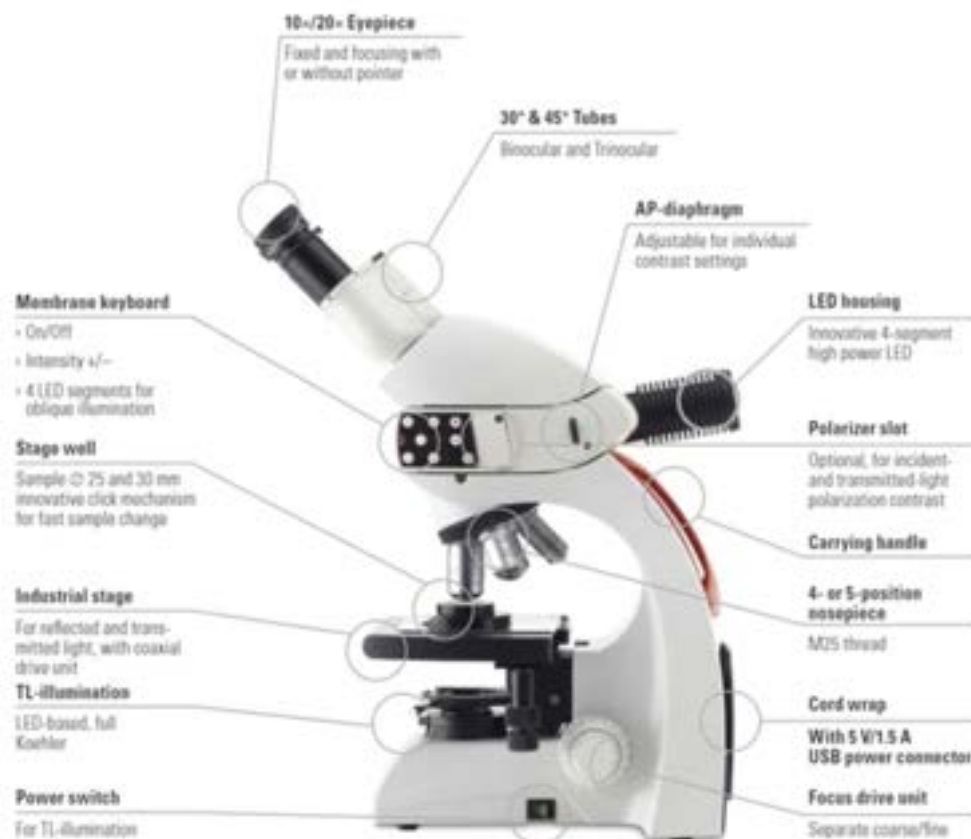

Fig. 12 The research light microscope with an upright stand (credits: https://www.indiamart.com/proddetail/microscope-binocular-dm750-leica-24170188933.html)

The preparation of a thin section for optical microscopy involves a meticulous and systematic process to ensure the sample's suitability for detailed microscopic examination. Initially, a representative sample of the rock, mineral, or material must be selected, ensuring that it is both dry and clean (Fig.13a). The sample is then cut using a diamond saw. During this analysis, the Struers Labotom-3 was used (Fig.13b). The cut surface must be smooth and flat. For this purpose, a polishing machine may be used, for example, Struers LaboPol-5 (Fig.13c).

Subsequently, the cut surface of the sample is thoroughly cleaned before it is mounted onto a glass slide using epoxy resin (Fig.13d). The sample must be firmly attached and level, with the epoxy allowed to cure completely, which may take several hours to overnight depending on the resin used. After curing, excess material is trimmed away.

The next phase involves grinding the sample to reduce its thickness further. This is achieved using a series of progressively finer abrasive discs or papers, starting with coarse grit and moving to finer grits, with continuous thickness checks aiming for approximately 100 microns. Once this thickness is achieved, the sample undergoes polishing using very fine abrasive compounds such as aluminum oxide or diamond paste. Polishing continues until the sample reaches the standard thickness of about 30 microns, ensuring proper light transmission for optical microscopy. Following the polishing stage, the thin section is meticulously cleaned to remove any remaining polishing compound or debris, using distilled water and a soft brush or ultrasonic cleaner.

The prepared thin section is labeled with pertinent information, including the sample name, location, and date, using a permanent marker or printed label for clarity and durability. Each of these components plays a crucial role in obtaining detailed and high-quality images. This microscope is also equipped with cameras to digitally capture and store images as needed. After the petrographic analysis each sample underwent digital image analysis. The ratio of binder, porosity and various aggregates were determined [21]. The quantification process utilized OM-TL scans of the thin sections as a reference. These scans were graphically processed using bichromatic thresholding after converting the RGB images to 8-bit grayscale. Porosity and aggregates were quantified separately. The binder fraction was estimated by subtracting the percentages of aggregates and voids from the total area. Sorting was based on the standard deviation (SD) between the mean measurements of fine and coarse aggregates [22]. To determine the grain size of the aggregate fraction the Wentworth scale was adopted [23].

<div align="center">Fig.13a</div>

<div align="center">Fig.13b</div>

<div align="center">Fig.13c</div>

<div align="center">Fig.13d</div>

Fig. 13 Preparation of the thin section for OM (photo by Sokolova E.)

The general table of groups was composed after performing the analysis mentioned above in order to demonstrate the common features of groups and outliers and systemize the obtained results (Table 4).

5.5 Digital image analysis (DIA)

Image analysis is the extraction of meaningful information from images; mainly from digital images by means of digital image processing techniques [24]. In archaeometry this analysis is usually performed by using the images obtained from the optical microscopy or SEM-EDS.

The software used for DIA is called ImageJ. It is a versatile tool for displaying, editing, analyzing, processing, saving, and printing images in various formats, including 8-bit color, grayscale, 16-bit integer, and 32-bit floating point. It supports multiple image file formats such as TIFF, PNG, GIF, JPEG, etc, along with raw formats. ImageJ can handle image stacks, perform multithreaded operations for efficiency on multi-CPU hardware, and supports a wide range of image processing functions. These functions include calculating area and pixel value statistics, measuring distances and angles, creating density histograms and line profile plots, and conducting geometric transformations like scaling, rotation, and flipping. It can also execute standard image processing tasks such as contrast manipulation, convolution, Fourier analysis, sharpening, smoothing, edge detection, and median filtering. The program can manage numerous images simultaneously, limited only by the available memory [25].

In digital imaging, a pixel is the smallest addressable element in a raster image, or the smallest addressable element in a dot matrix display device. In most digital display devices, pixels are the smallest element that can be manipulated through software [26].

To perform the analysis of a picture taken during the optical microscopy examination, it is necessary to change its format to the 8-bit one. Each pixel has a value included between 0 (black) and 255 (white). After that, the brightness, contrast and color balance are adjusted in order to obtain the best quality of the image. Then, manual thresholding is used to select a range of values from the frequency histogram - it is one of the main methods of image segmentation. Finally, it is possible to analyze the particles and obtain the summary of the percentage of the aggregates and pores. This data is crucial in order to be able to define the binder to aggregate ratio. This ratio is used to determine the type of mortar (e.g. lean, fat).

After performing the analysis, a ternary plot was elaborated, for graphically displaying the results of DIA acquisitions, reporting binder, aggregate and porosities percentages on each bar. This type of diagram is used to represent the proportions of three different components in a rock or mineral sample. These plots are valuable for visualizing the composition of minerals and rocks that are formed by the combination of three primary constituents (Fig. 35).

Chapter 6. Results

The results chapter presents a thorough analysis and interpretation of data collected through experimental investigations. It synthesizes findings from a range of analytical techniques such as X-ray powder diffraction (XRPD), colorimetry, optical microscopy, and SEM-EDS. These methods were utilized to characterize and clarify the mineralogical composition, chemical properties, and visual characteristics of the samples under examination.

6.1 XRPD

The XRPD analysis facilitated the identification of the mineralogical composition of the samples, including the presence of amorphous phases.

The samples contain a mixture of aggregates (silicate and carbonate clasts). However, predominant minerals observed across all samples were calcite and dolomite, as indicated in Table 4. To further analyze the data, principal component analysis (PCA) was conducted to simplify and visualize the complex dataset. PCA transforms correlated variables into a smaller set of uncorrelated principal components, reducing dimensionality and enhancing the clarity of patterns, trends, and outliers in high-dimensional data.

The biplot obtained from PCA analysis (Fig. 14) reveals that samples PREP_11, PREP_09, PREP_02, PREP_07, and PREP_03 (PREP shortened to P in the biplot) exhibit characteristics that classify them as outliers. This observation aligns with the X-ray powder diffraction (XRPD) data presented in Table 4, showing these samples contain a significant amount of amorphous phases and higher levels of diopside or aragonite. These findings suggest the possible presence of cocciopesto components within these samples, an inference that will be further discussed in the subsequent results of the colorimetry analysis.

The sample WM_14 also seems to be an outlier as it has a more significant amount of quartz. The samples INT_05E, INT_04A and INT_O5D (INT shortened to I in the biplot) fall out of the common group as well due to high amorphous phase content.
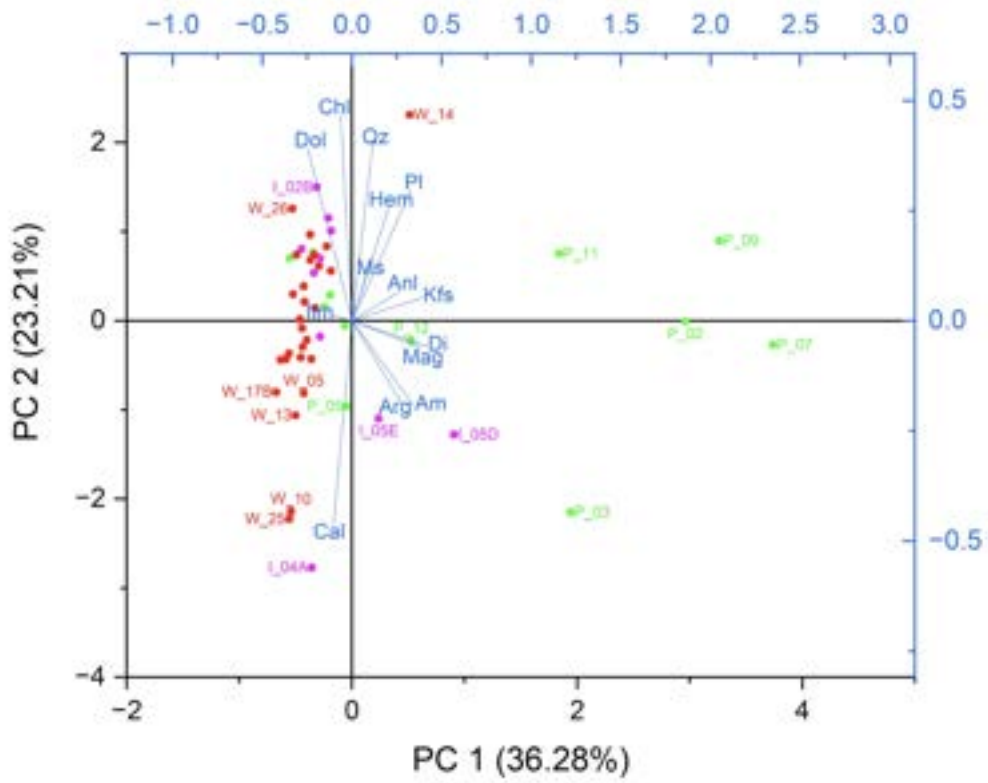
Fig. 14 PCA biplot of all the analyzed samples

A subset biplot without the most evident outliers was created later (Fig.15). It is possible to distinguish two big groups, a smaller one and four outliers.
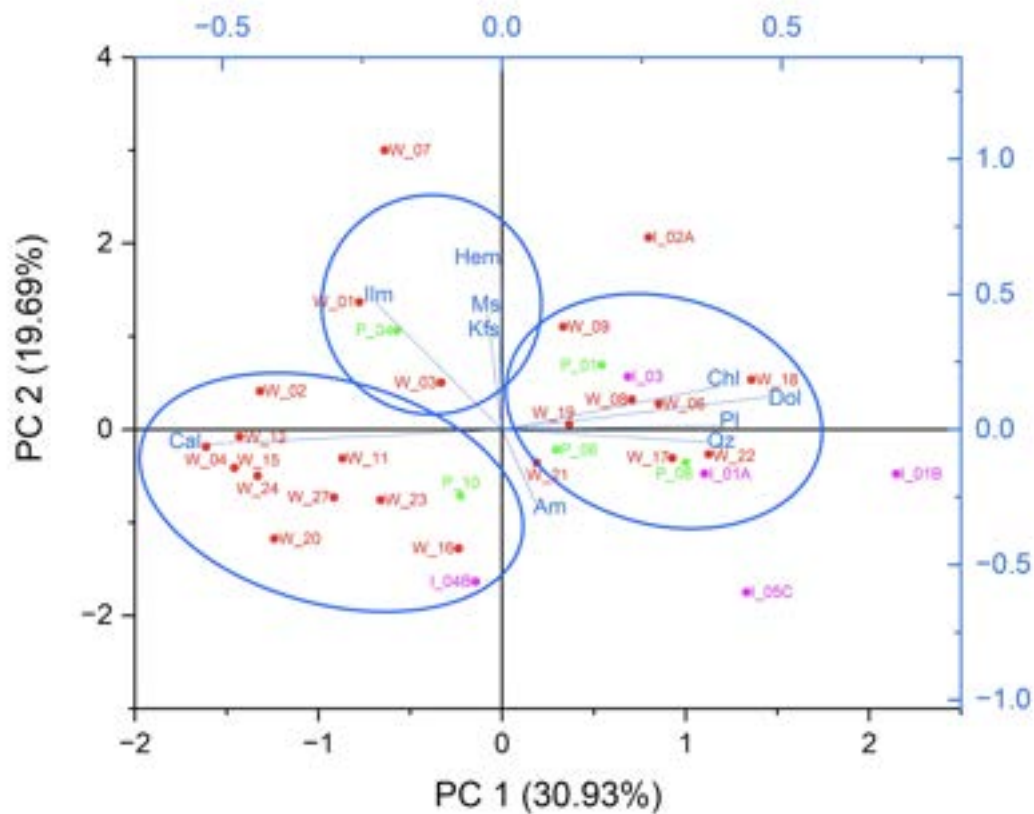
Fig. 15 Subset biplot excluding outliers

As the primary objective of this study is to analyze the composition of the wall mortars, a detailed discussion will follow.

The wall mortar samples are composed of the mix of the aggregates (silicate and carbonates), however the two predominant phases identified in all wall mortar compositions are calcite and dolomite.

Calcite, a mineral composed of calcium carbonate ($CaCO_3$), crystallizes in the trigonal system. It is ubiquitously found in sedimentary rocks such as limestone and constitutes a major component of marine shells and corals. In the context of wall mortars, calcite frequently forms through the carbonation of lime (calcium hydroxide) in the presence of atmospheric CO_2, resulting in the development of a strong, durable matrix [27].

Dolomite, comprising calcium magnesium carbonate ($CaMg(CO_3)_2$), also crystallizes in the trigonal system. It is predominantly found in sedimentary rocks known as dolostones and can originate from the alteration of limestone through the process of dolomitization. In mortars, dolomite is typically introduced via the use of dolomitic sand, derived from weathering or comminution of dolostone. The presence of dolomite can significantly enhance the durability and strength of the mortar, especially in environments subject to sulfate attack [28].

The remaining composition is constituted by quartz, plagioclase (albite), K-feldspars (microcline), chlorite (clinochlore), micas/illite (muscovite), hematite, and ilmenite.

41

Minerals such as aragonite, diopside, magnetite, and analcime are either present in minimal amounts or completely absent.

The PC analysis was carried out on wall mortars samples separately. In the biplot PC1/PC2 (fig. 16), it is evident that the samples WM_25, WM_10, WM_07 and WM_14 are the outliers. According to the results of the XRPD analysis in table 4, WM_10 and WM_25 have the highest content of calcite and WM_14 has the highest content of quartz.
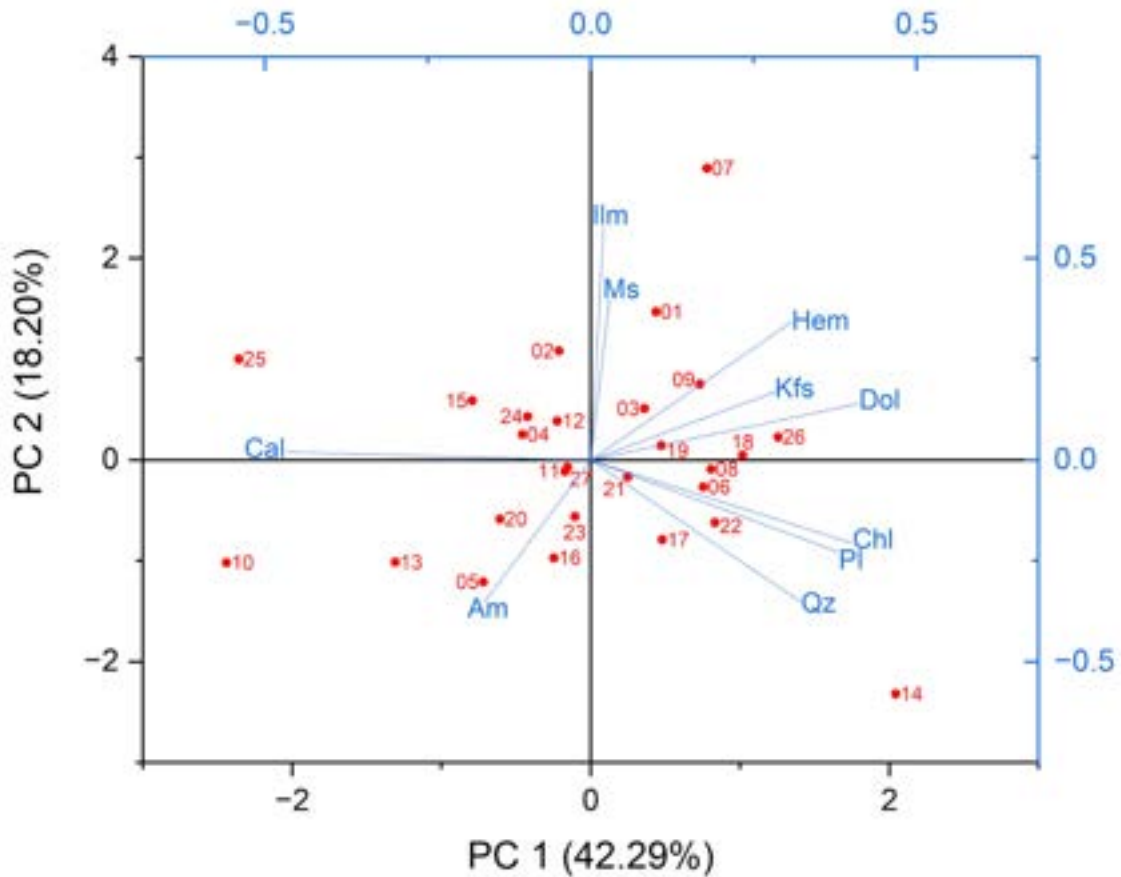

Fig. 16 Wall mortars biplot PC1/PC2

A biplot PC1/PC3 was created later (Fig.17). The samples can be grouped into one big set and several smaller ones, however the WM_14 is still an outlier as it has the highest quartz content out of all wall mortar samples.
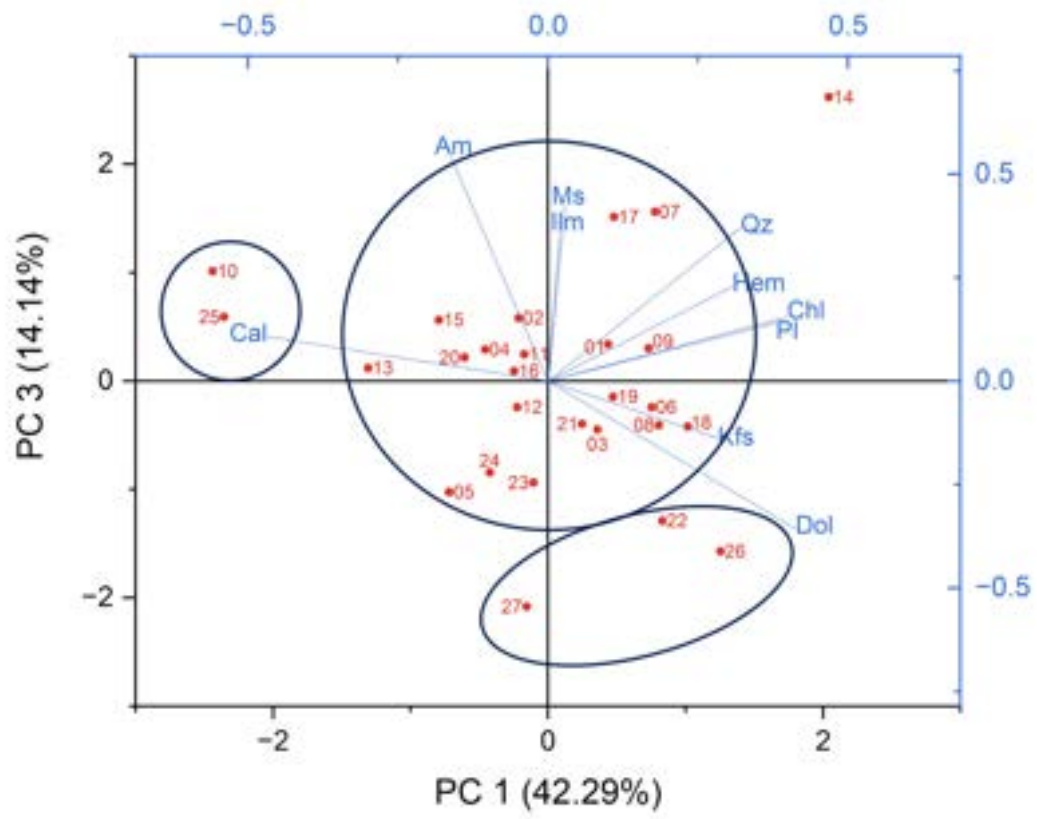
Fig. 17 Wall mortars biplot PC1/PC3

Table 4. The mineral composition of the samples obtained from XRPD analysis

Sample	Strat.unit	Description	Colorimetric parameters							Mineralogical composition													
			L*	a*	b*	Color	R	G	B	Calcite	Aragonite	Dolomite	Quartz	Plagioclase	K-feldspar	Micas/Illite	Chlorite	Diopside	Analcime	Hematite	Magnetite	Ilmenite	Amorphous
BB_INT_01A		Rinzaffo	84.0	1.0	8.3		218	208	194	36.75	0.00	42.44	7.05	1.99	0.32	0.33	1.20	0.00	0.00	0.56	0.00	0.32	9.00
BB_INT_01B		Arriccio+intonachino	85.4	1.3	8.8		223	212	197	31.46	0.00	49.32	7.31	1.94	0.70	0.39	1.39	0.00	0.00	0.54	0.00	0.18	6.73
BB_INT_02A		Rinzaffo	88.0	0.9	7.3		229	220	207	36.11	0.00	45.74	5.8	1.82	0.89	0.70	1.27	0.00	0.00	0.73	0.00	0.38	6.51
BB_INT_02B		Arriccio	86.9	1.1	7.7		226	216	203	27.77	0.00	53.50	7.44	1.77	0.67	0.67	1.41	0.00	0.00	0.63	0.00	0.34	5.76
BB_INT_02C		Intonachino	95.0	0.7	3.9		245	240	233	91.76	0.00	0.56	1.07	0.00	0.00	0.00	0.00	0.00	0.00	0.00	0.00	0.38	6.20
BB_INT_03	USM3	Intonaco	88.5	1.0	7.7		231	221	208	40.62	0.00	42.88	6.33	1.76	0.37	0.42	1.39	0.00	0.00	0.62	0.00	0.35	5.21
BB_INT_04_A	US104	Plaster, first layer								65.91	2.21	12.70	1.71	0.82	0.08	0.12	0.42	0.00	0.00	0.19	0.00	0.36	15.42
BB_INT_04_B	US104	Plaster, second layer								39.80	0.00	37.97	4.00	1.50	0.36	0.42	1.07	0.00	0.00	0.45	0.00	0.26	14.13
BB_INT_05_C	USM101	Plaster, third layer								32.55	0.00	44.78	6.61	1.72	0.21	0.33	1.22	0.00	0.00	0.42	0.00	0.25	11.86
BB_INT_05_D	USM101	Plaster, fourth layer								42.68	0.00	19.14	4.68	1.24	1.37	0.40	0.21	3.74	0.00	0.68	0.00	0.17	25.64
BB_INT_05_E	USM101	Plaster, paint layer								52.91	0.00	20.32	3.53	1.40	1.10	0.49	0.62	0.00	0.00	0.62	0.00	0.27	18.70
BB_PREP_01	US14	Base concrete of the floor	88.1	1.0	6.9		229	220	208	40.39	0.00	42.08	6.56	1.60	0.46	0.50	1.30	0.00	0.00	0.67	0.00	0.32	6.08
BB_PREP_02	US1002	Cocciopesto floor	83.0	4.3	12.4		225	203	184	32.55	2.51	12.12	7.97	2.76	3.77	0.00	1.24	11.89	0.66	0.53	0.28	0.43	23.24
BB_PREP_03	US8	Upper floor preparation	87.0	3.4	11.7		234	215	196	54.66	2.66	3.39	5.33	1.26	1.30	0.43	0.38	8.66	0.00	0.50	0.56	0.29	20.53
BB_PREP_04	US12	Upper floor preparation	87.4	2.0	8.1		230	217	204	47.40	0.00	31.88	5.86	1.62	0.85	0.63	1.28	0.00	0.00	0.62	0.00	0.41	9.40
BB_PREP_05	US28	Base concrete of the floor	88.3	1.4	8.3		231	220	206	57.22	2.93	23.37	5.11	1.25	0.61	0.29	0.99	0.00	0.00	0.54	0.00	0.37	7.28
BB_PREP_06	US156	Base concrete of the floor	84.7	1.5	8.4		221	210	196	35.91	0.68	44.47	7.25	1.75	0.36	0.50	0.55	0.00	0.00	0.54	0.00	0.36	7.57

Sample	Strat.unit	Description	Colorimetric parameters							Mineralogical composition													
			L*	a*	b*	Color	R	G	B	Calcite	Aragonite	Dolomite	Quartz	Plagioclase	K-feldspar	Micas/Illite	Chlorite	Diopside	Analcime	Hematite	Magnetite	Ilmenite	Amorphous
BB_PREP_07	US124	Cocciopesto floor	84.5	5.0	14.4		231	207	184	35.34	4.52	7.07	7.09	4.13	2.67	0.84	0.82	12.50	0.00	0.75	0.55	0.26	23.40
BB_PREP_08	US157	Base concrete of the floor	88.8	1.3	8.1		232	222	208	38.91	0.00	44.83	6.65	1.97	0.31	0.27	1.31	0.00	0.00	0.46	0.00	0.36	4.88
BB_PREP_08_S		Calcination relict inside BB_PREP_08	95.9	0.8	3.5		248	243	237	93.76	0.00	2.25	1.02	0.00	0.00	0.00	0.00	0.00	0.00	0.00	0.00	0.19	2.75
BB_PREP_09	US124	Cocciopesto floor	85.3	3.1	12.5		229	210	190	30.40	0.00	26.26	6.75	3.79	2.52	0.29	1.00	9.83	1.61	0.71	0.64	0.28	15.85
BB_PREP_10	US143	Base concrete of the floor	88.8	1.9	8.8		234	221	206	44.40	0.00	36.23	6.24	1.49	1.26	0.10	0.91	1.59	0.00	0.55	0.00	0.22	6.95
BB_PREP_11	US126	Upper floor preparation	81.4	7.7	15.0		228	197	175	51.67	0.00	8.18	9.71	3.33	2.65	1.13	0.94	3.24	0.00	1.06	0.00	0.24	17.80
BB_PREP_12	US125	Mortar layer of the mosaic tesserae	85.1	5.5	11.9		232	208	190	59.31	0.00	15.93	6.39	2.02	1.85	0.84	0.86	0.00	0.00	0.80	0.00	0.35	11.61
BB_WM_01		Bedding mortar	90.1	1.0	6.7		234	225	214	45.31	0.00	38.47	4.62	1.51	0.94	0.42	1.02	0.00	0.00	0.68	0.00	0.42	6.58
BB_WM_02		Bedding mortar	90.2	1.0	6.6		234	226	214	53.50	0.00	32.13	4.27	2.04	0.33	0.36	0.85	0.00	0.00	0.61	0.00	0.44	5.43
BB_WM_03		Bedding mortar	89.2	1.0	7.2		232	223	211	43.48	0.00	41.04	5.10	1.46	0.73	0.33	1.06	0.00	0.00	0.62	0.00	0.35	5.78
BB_WM_04		Bedding mortar	90.2	0.9	5.9		234	226	216	52.04	0.00	31.35	4.55	1.13	0.51	0.37	1.00	0.00	0.00	0.59	0.00	0.35	8.05
BB_WM_05	USM4	Bedding mortar	90.9	1.0	6.4		236	228	217	54.89	0.00	29.12	4.30	1.52	0.67	0.13	0.86	0.00	0.00	0.40	0.00	0.27	7.80
BB_WM_06	USM3	Bedding mortar	87.1	1.1	7.9		227	217	203	36.4	0.00	45.26	6.40	1.65	0.58	0.27	1.22	0.00	0.00	0.65	0.00	0.32	7.21
BB_WM_07	USM2	Bedding mortar (upper level)	89.1	1.0	7.7		232	223	209	43.96	0.83	38.58	6.26	1.31	0.94	0.95	1.14	0.00	0.00	0.75	0.00	0.47	4.77
BB_WM_08	USM2	Bedding mortar (lower level)	88.3	1.0	7.8		230	220	207	36.66	0.00	44.60	6.28	1.66	0.92	0.24	1.17	0.00	0.00	0.59	0.00	0.34	7.48
BB_WM_09	USM5	Bedding mortar	89.2	0.9	7.8		232	223	209	39.80	0.00	42.95	5.85	1.55	0.75	0.57	1.30	0.00	0.00	0.61	0.00	0.37	6.22
BB_WM_10	US18	Bedding mortar	89.5	1.1	6.1		232	224	213	77.82	0.00	4.28	3.89	0.78	0.23	0.19	0.78	0.00	0.00	0.38	0.00	0.34	11.26
BB_WM_11	USM6	Bedding mortar	89.4	1.0	7.0		232	223	211	49.31	0.00	33.33	5.52	1.40	0.46	0.32	1.12	0.00	0.00	0.56	0.00	0.35	7.59

Sample	Strat.unit	Description	Colorimetric parameters							Mineralogical composition													
			L*	a*	b*	Color	R	G	B	Calcite	Aragonite	Dolomite	Quartz	Plagioclase	K-feldspar	Micas/Illite	Chlorite	Diopside	Analcime	Hematite	Magnetite	Ilmenite	Amorphous
BB_WM_12		Bedding mortar	90.0	0.9	6.5		234	225	214	49.81	0.00	33.37	4.85	1.24	0.93	0.32	0.84	0.00	0.00	0.55	0.00	0.35	7.69
BB_WM_13		Bedding mortar	91.1	0.9	6.3		237	228	218	58.58	0.00	23.8	4.39	0.94	0.35	0.36	0.9	0.00	0.00	0.42	0.00	0.28	9.93
BB_WM_14	US116	Lean concrete over the foundation of the wall	82.6	5.3	12.2		225	201	183	32.20	0.00	33.43	16.94	3.16	0.78	0.49	1.51	0.00	0.00	0.63	0.00	0.30	10.52
BB_WM_15	USM102	Foundation mortar	88.6	1.3	7.0		231	221	209	48.36	0.00	35.50	5.23	1.03	0.25	0.84	0.79	0.00	0.00	0.41	0.00	0.35	7.19
BB_WM_16	US132	Lean concrete over the foundation of the wall	86.9	1.3	8.2		227	216	202	46.79	0.00	34.07	7.37	1.58	0.34	0.30	1.07	0.00	0.00	0.41	0.00	0.33	7.67
BB_WM_17	USM102	Mortar at the base of the wall	87.6	1.5	8.9		230	218	203	43.40	0.00	32.83	10.19	1.94	0.51	0.63	1.41	0.00	0.00	0.42	0.00	0.36	8.27
BB_WM_17_B	USM102	Recycled plaster inside BB_WM_17	90.7	1.1	6.2		236	227	217	56.68	0.00	29.95	4.99	1.25	0.26	0.09	0.81	0.00	0.00	0.45	0.00	0.33	5.14
BB_WM_18	USM101	Foundation mortar	86.0	1.4	8.3		224	214	200	34.10	0.00	48.45	6.87	1.88	0.73	0.45	1.27	0.00	0.00	0.53	0.00	0.34	5.33
BB_WM_19	USM101	Mortar at the base of the wall	89.2	1.3	8.0		233	223	209	42.47	0.00	41.38	5.56	2.19	0.47	0.21	1.10	0.00	0.00	0.54	0.00	0.40	5.62
BB_WM_20	USM101	Foundation mortar	88.8	1.5	7.9		232	221	208	52.87	0.00	29.73	5.90	1.34	0.23	0.18	1.08	0.00	0.00	0.48	0.00	0.36	7.78
BB_WM_21	USM104	Foundation mortar	88.8	1.4	8.2		232	221	207	41.15	0.00	42.06	5.99	1.59	0.56	0.31	1.16	0.00	0.00	0.45	0.00	0.36	6.33
BB_WM_22	US400	Bedding mortar	89.0	1.0	7.8		232	222	209	36.41	0.00	47.15	6.55	1.64	0.88	0.26	1.38	0.00	0.00	0.42	0.00	0.31	5.00
BB_WM_23	US201	Bedding mortar	89.9	1.0	6.8		234	225	213	47.83	0.00	36.32	5.08	1.51	0.77	0.33	0.97	0.00	0.00	0.46	0.00	0.28	6.46
BB_WM_24	US200	Bedding mortar	87.7	1.0	6.4		227	219	208	52.26	0.00	35.31	4.97	1.52	0.45	0.29	0.81	0.00	0.00	0.46	0.00	0.37	3.57
BB_WM_25	US202	Bedding mortar	88.2	1.0	5.7		228	220	211	73.48	0.00	13.23	3.44	0.94	0.43	0.77	0.15	0.00	0.00	0.33	0.00	0.37	6.86
BB_WM_26	US317	Bedding mortar	85.8	1.3	8.3		224	213	199	32.56	0.00	54.59	7.85	2.03	0.49	0.45	1.17	0.00	0.00	0.54	0.00	0.31	0.02
BB_WM_27	USM300	Bedding mortar	85.7	1.4	7.7		223	213	200	50.54	0.00	37.93	5.89	1.54	0.80	0.26	0.68	0.00	0.00	0.42	0.00	0.29	1.66

6.2 Colorimetry

The colorimetric analysis was performed on the majority of the samples taken (Table 5). In addition, the principal component analysis was performed in order to obtain statistical data and interpret the results in a more precise way (Fig.18).

The most noticeable outliers are samples INT_02C, INT_01A (INT shortened to I) and WM_14. The samples of the preparatory layer (P_11, P_03, P_12, P_09, P_02, P_07) can be grouped together. This position of the samples on the statistical biplot is correlated with the data in table 5, as their colorimetric parameters (L A B/ RGB) are more diverse than any other set of samples.
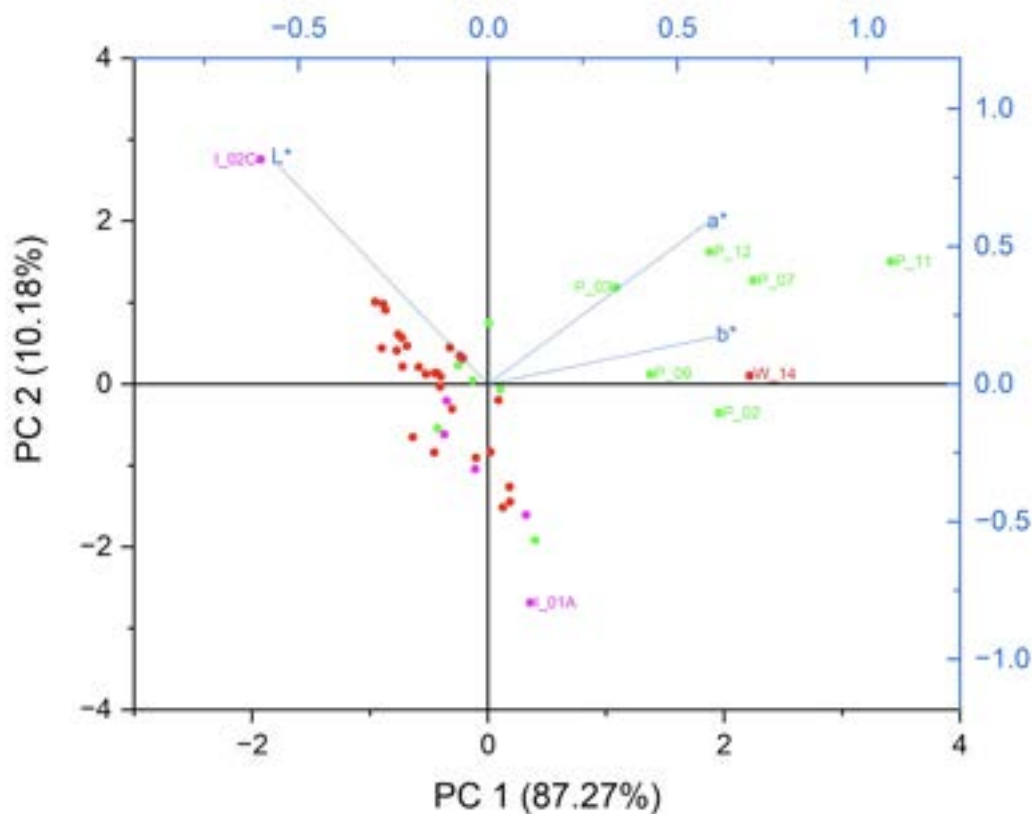
Fig. 18 PCA biplot colorimetry

A subset excluding the combined group of PREP samples, as well as other three outliers, was created (Fig.19). Here three groups can be distinguished, together with two outliers PREP_10 and PREP_04.
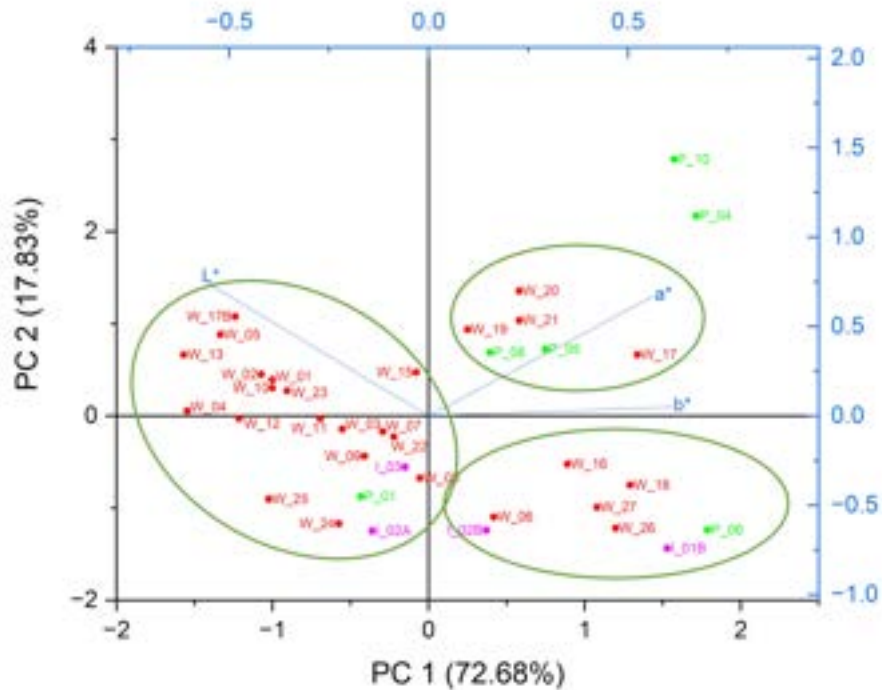
Fig. 19 PC1/PC2 biplot excluding outliers, colorimetry

Later the biplot of wall mortar samples was created separately as they are the main object of the research (Fig.20). Here, the sample WM_14 is the most evident outlier. The reason for this is evident in the table with the colorimetry results, as it has the most reddish shade out of all the wall mortar samples.
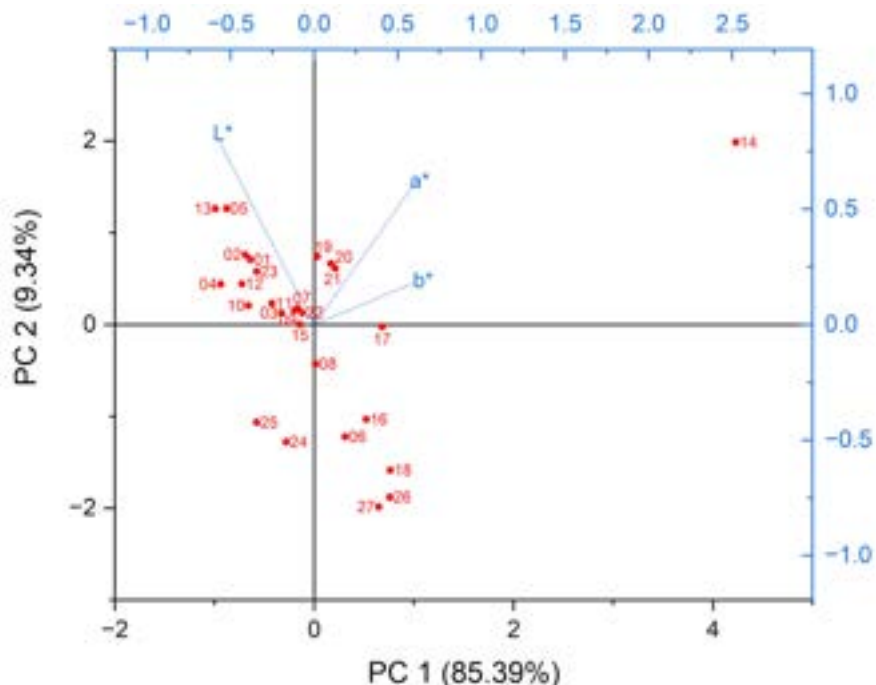
Fig. 20 Wall mortars biplot PCA, colorimetry

A subset excluding the WM_14 was created (Fig.21) and here we can observe four groups, two of which consist of a bigger number of samples.
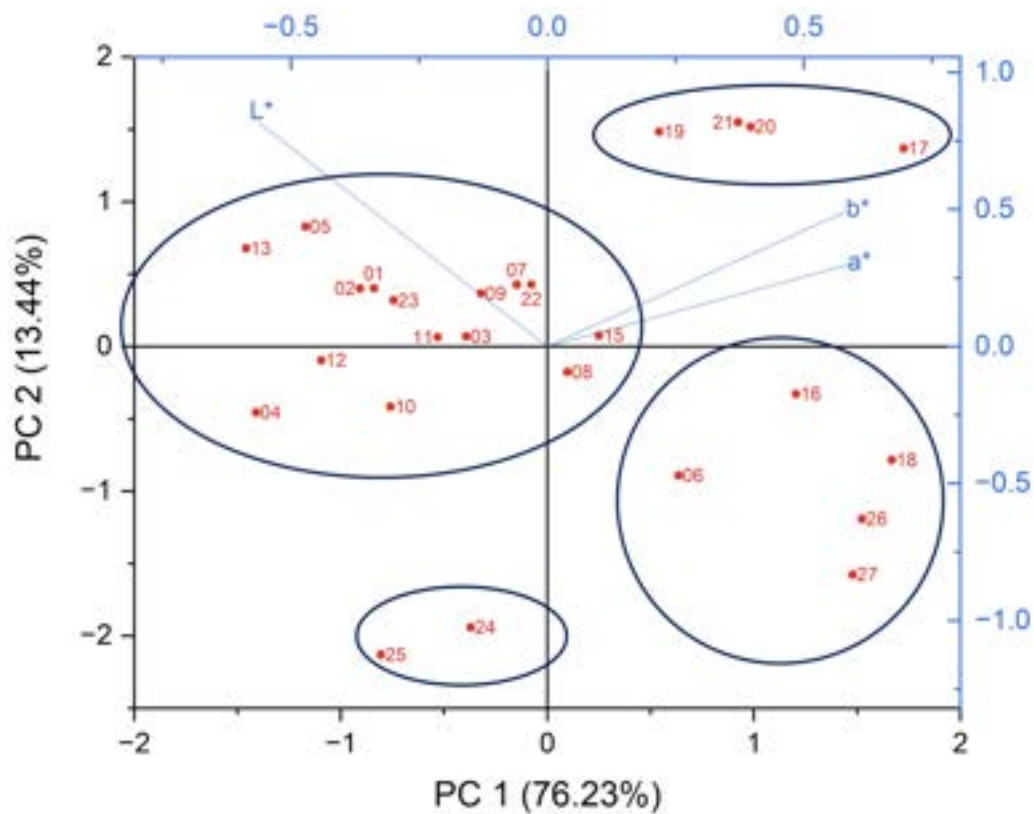
Fig. 21 Wall mortars subset biplot excluding the outlier WM_14

Table 5. Colorimetry analysis results

Sample	Strat.unit	Description	Colorimetric parameters						
			L*	a*	b*	Color	R	G	B
BB_INT_01A		Rinzaffo	84.0	1.0	8.3		218	208	194
BB_INT_01B		Arriccio+intonachino	85.4	1.3	8.8		223	212	197
BB_INT_02A		Rinzaffo	88.0	0.9	7.3		229	220	207
BB_INT_02B		Arriccio	86.9	1.1	7.7		226	216	203
BB_INT_02C		Intonachino	95.0	0.7	3.9		245	240	233
BB_INT_03	USM3	Intonaco	88.5	1.0	7.7		231	221	208
BB_INT_04_A	US104	Plaster, first layer							
BB_INT_04_B	US104	Plaster, second layer							
BB_INT_05_C	USM101	Plaster, third layer							
BB_INT_05_D	USM101	Plaster, fourth layer							
BB_INT_05_E	USM101	Plaster, paint layer							
BB_PREP_01	US14	Base concrete of the floor	88.1	1.0	6.9		229	220	208
BB_PREP_02	US1002	Cocciopesto floor	83.0	4.3	12.4		225	203	184

Sample	Strat.unit	Description	Colorimetric parameters						
			L*	a*	b*	Color	R	G	B
BB_PREP_03	US8	Upper floor preparation	87.0	3.4	11.7		234	215	196
BB_PREP_04	US12	Upper floor preparation	87.4	2.0	8.1		230	217	204
BB_PREP_05	US28	Base concrete of the floor	88.3	1.4	8.3		231	220	206
BB_PREP_06	US156	Base concrete of the floor	84.7	1.5	8.4		221	210	196
BB_PREP_07	US124	Cocciopesto floor	84.5	5.0	14.4		231	207	184
BB_PREP_08	US157	Base concrete of the floor	88.8	1.3	8.1		232	222	208
BB_PREP_08_S		Calcination relict inside BB_PREP_08	95.9	0.8	3.5		248	243	237
BB_PREP_09	US124	Cocciopesto floor	85.3	3.1	12.5		229	210	190
BB_PREP_10	US143	Base concrete of the floor	88.8	1.9	8.8		234	221	206
BB_PREP_11	US126	Upper floor preparation	81.4	7.7	15.0		228	197	175
BB_PREP_12	US125	Mortar layer of the mosaic tesserae	85.1	5.5	11.9		232	208	190
BB_WM_01		Bedding mortar	90.1	1.0	6.7		234	225	214
BB_WM_02		Bedding mortar	90.2	1.0	6.6		234	226	214
BB_WM_03		Bedding mortar	89.2	1.0	7.2		232	223	211
BB_WM_04		Bedding mortar	90.2	0.9	5.9		234	226	216
BB_WM_05	USM4	Bedding mortar	90.9	1.0	6.4		236	228	217
BB_WM_06	USM3	Bedding mortar	87.1	1.1	7.9		227	217	203
BB_WM_07	USM2	Bedding mortar (upper level)	89.1	1.0	7.7		232	223	209
BB_WM_08	USM2	Bedding mortar (lower level)	88.3	1.0	7.8		230	220	207
BB_WM_09	USM5	Bedding mortar	89.2	0.9	7.8		232	223	209
BB_WM_10	US18	Bedding mortar	89.5	1.1	6.1		232	224	213
BB_WM_11	USM6	Bedding mortar	89.4	1.0	7.0		232	223	211
BB_WM_12		Bedding mortar	90.0	0.9	6.5		234	225	214
BB_WM_13		Bedding mortar	91.1	0.9	6.3		237	228	218
BB_WM_14	US116	Lean concrete over the foundation of the wall	82.6	5.3	12.2		225	201	183
BB_WM_15	USM102	Foundation mortar	88.6	1.3	7.0		231	221	209
BB_WM_16	US132	Lean concrete over the foundation of the wall	86.9	1.3	8.2		227	216	202

Sample	Strat.unit	Description	Colorimetric parameters						
			L*	a*	b*	Color	R	G	B
BB_WM_17	USM102	Mortar at the base of the wall	87.6	1.5	8.9		230	218	203
BB_WM_17_B	USM102	Recycled plaster inside BB_WM_17	90.7	1.1	6.2		236	227	217
BB_WM_18	USM101	Foundation mortar	86.0	1.4	8.3		224	214	200
BB_WM_19	USM101	Mortar at the base of the wall	89.2	1.3	8.0		233	223	209
BB_WM_20	USM101	Foundation mortar	88.8	1.5	7.9		232	221	208
BB_WM_21	USM104	Foundation mortar	88.8	1.4	8.2		232	221	207
BB_WM_22	US400	Bedding mortar	89.0	1.0	7.8		232	222	209
BB_WM_23	US201	Bedding mortar	89.9	1.0	6.8		234	225	213
BB_WM_24	US200	Bedding mortar	87.7	1.0	6.4		227	219	208
BB_WM_25	US202	Bedding mortar	88.2	1.0	5.7		228	220	211
BB_WM_26	US317	Bedding mortar	85.8	1.3	8.3		224	213	199
BB_WM_27	USM300	Bedding mortar	85.7	1.4	7.7		223	213	200

6.3 Optical microscopy

During the petrographic investigation detailed in this chapter, the analysis revealed three distinct groups of rock samples, each characterized by unique mineralogical and textural features (Table 6). Additionally, two outliers were identified, standing apart from the primary groups due to their peculiar features and characteristics.

Group 1. WM_01, WM_02, WM_03, WM_04, WM_05, WM_06, WM_07, WM_08, WM_09, WM_10, WM_12, WM_13, WM_19, WM_20, WM_23, WM_24, WM_25.

The samples of this group are characterized as lime-based mortars. The binder is micritic and homogeneous with high birefringence colors - which means that it is completely carbonated. Lumps are present in a big number which is a sign of lower quality mixing. The lumps are shown in fig.22a-22f. Voids are mainly vughs (fig.22c,22d) but sometimes vesicles and channels are noticeable in low numbers (fig.22e, 22f). Aggregates are mostly represented as medium sands according to the Wentworth scale, but a little percentage of fine sands is present as well. The binder to aggregate ratio = 2:1, which means that the mortar can be described as fat. Most aggregates belong to carbonate clasts (limestones, dolostones). Quartz and chert are also present, and little amounts of opaque minerals and feldspars are distinguished as well (fig.22a, 22b).
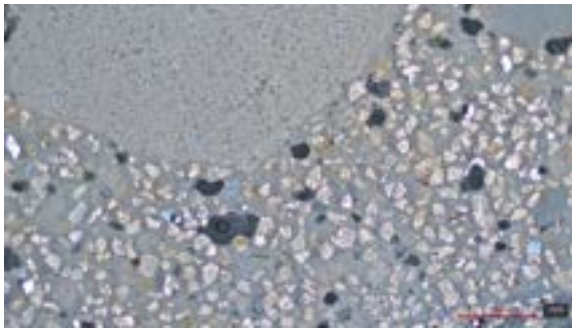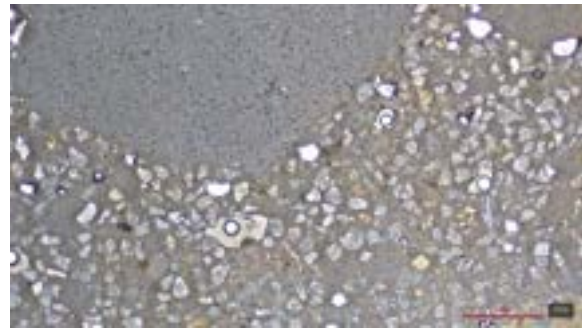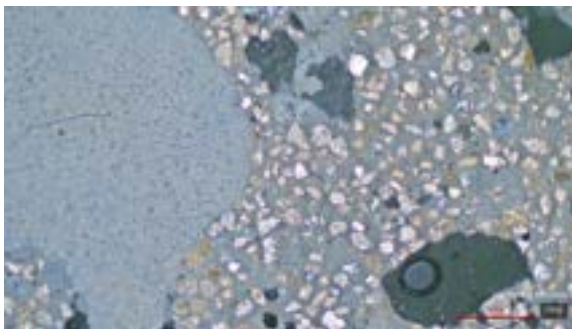
Fig.22a

Fig.22b

Fig.22c

Fig.22d
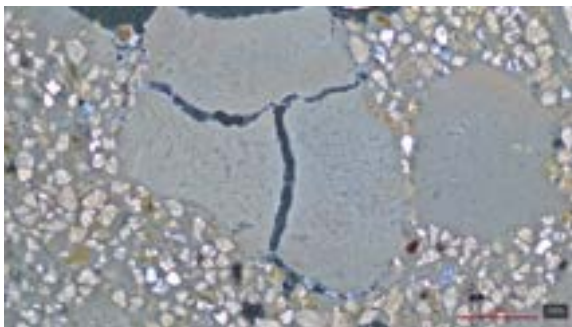
Fig.22e
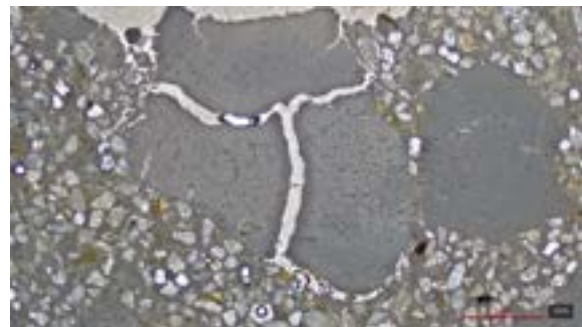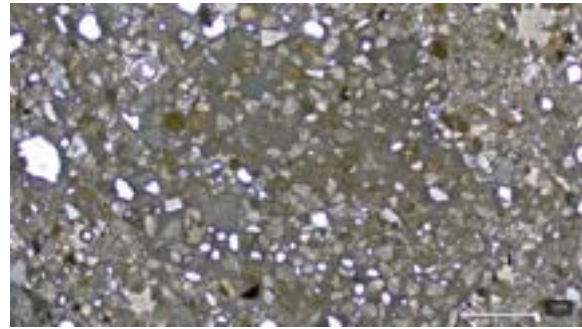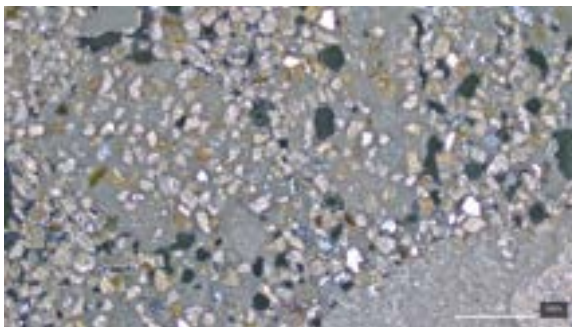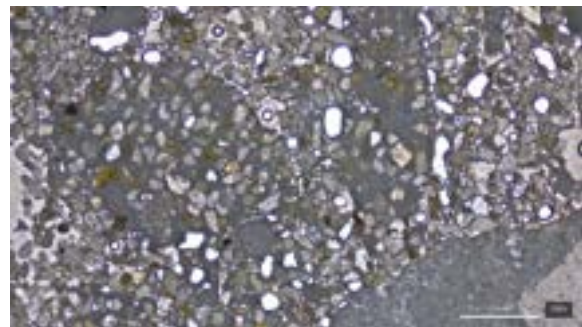

Fig.22f

Fig. 22 Micrographs of samples of Group 1; a-b) the general composition of sample WM_04 (cross and plane polars, scale bar = 1 mm); c-d) the general composition of sample WM_13, with evident pores of the vughs type (cross and plane polars, scale bar = 1 mm); e-f) the general composition of sample WM_23, with evident pores of the vughs type, and planar voids pores within a lime lump.

Group 2. WM_14, WM_16, WM_17.

The samples of this group are characterized as lime-based mortars. The binder is micritic and homogeneous with high birefringence colors. Lumps are absent or present in very low numbers. Voids are mainly vughs, and they make up only 9% of the sample composition. The main characteristic of this group is the presence of fine gravel (Wentworth, 1922). Fine aggregates are represented by medium to fine sands, comprising carbonate clasts, sandstones (fig. 23a, 23b), big pieces of chert (fig. 23c, 23d), small amounts of mica, feldspars, chlorites. Binder to aggregate ratio is equal to 2:3.

Cross polars   Plane polars
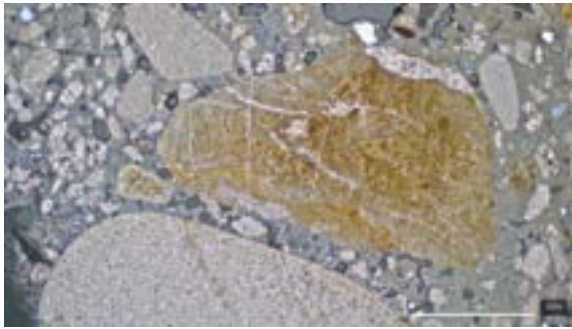
Fig.23a
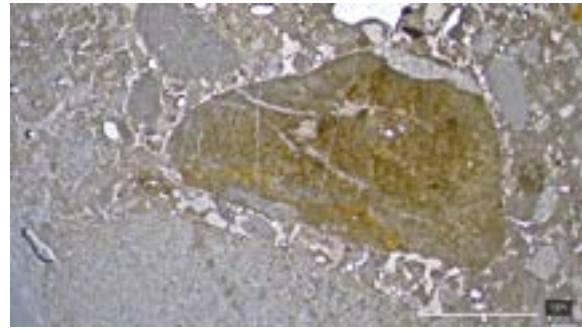
Fig.23b
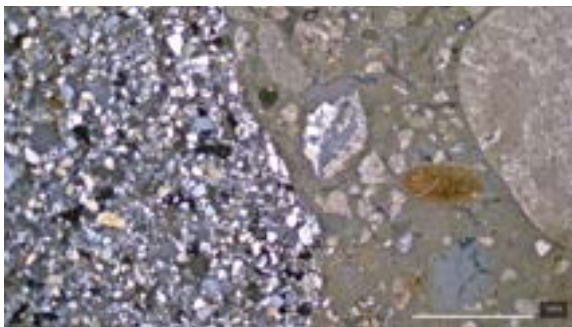
Fig.23c
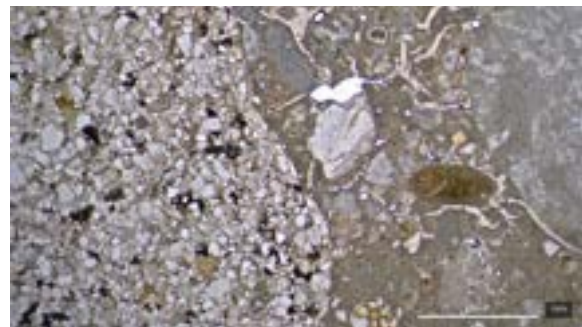
Fig.23d

Fig. 23 Micrographs of samples of Group 2; a-b) the general composition of sample WM_16 with sandstones as aggregates (cross and plane polars, scale bar = 1 mm); c-d) the general composition of sample WM_17, with evident inclusions of chert (cross and plane polars, scale bar = 1 mm);

Group 3. This group consists of 2 samples - WM_26, WM_27.

The samples of this group are characterized as lime-based mortars. The binder is micritic and homogeneous with high birefringence colors. Voids are mainly vughs, they occupy 11-15% of the whole sample composition. In particular, this group is connoted by the presence of angular chips of stones and pieces of reused mortars (Fig.24a-24d). Aggregates belong to the medium sands class (250-350µ) (Wentworth, 1922), mostly consisting of carbonate clasts. There are clasts of quartz and chert in lower concentrations, together with scarce sandstone, clay pellets and opaque minerals.

Cross polars   Plane polars
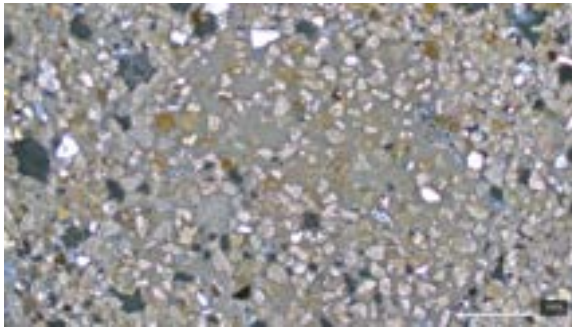
Fig.24a   Fig.24b
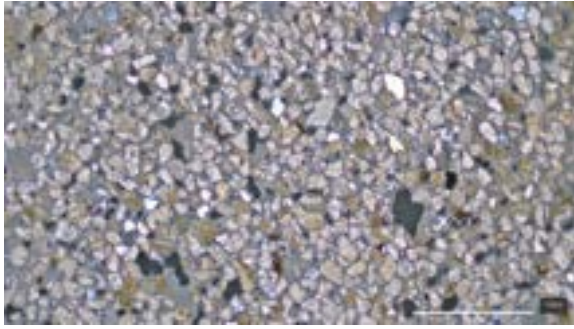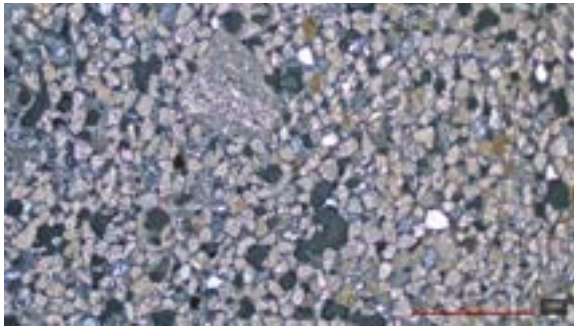

Fig.24c   Fig.24d

Fig. 24 Micrographs of samples of Group 3; a-b) the general composition of sample WM_26 (cross and plane polars, scale bar = 1 mm); c-d) the general composition of sample WM_27, with pieces of reused mortar (cross and plane polars, scale bar = 1 mm);

Outliers. There are also two samples which have different features that can't be matched with the three groups mentioned above. These are the samples WM_11 and WM_22.

WM_11 is characterized as a lime-based mortar. The binder is micritic and homogeneous with high birefringence colors. Lumps are present but in a small percentage. Voids are mainly vughs. The mean size of the aggregates is 698.5 μm which fits the coarse sands size range from 500 to 710 μm (fig.25a). Binder to aggregate proportion is 1:1, indicative of a leaner mortar (fig.25b). Aggregates are represented by carbonate clasts, quartz, low presence of opaque minerals, sandstone, mica, feldspars

WM_22 is characterized as a lime-based mortar. The binder is micritic and homogeneous with high birefringence colors. Lumps are absent (fig.25c). Voids are mainly vughs and they make up 19% of the whole sample composition. Binder to aggregate proportion is 1:2, which means that the mortar can be described as lean. The mean size of aggregates is 259.1μm and, according to the Wentworth scale, is considered as medium sands (size range from 250 to 350μ). Aggregates consist mostly of carbonate clasts, with little presence of sandstones, quartz, chert, mica and opaque minerals.

Cross polars   Plane polars
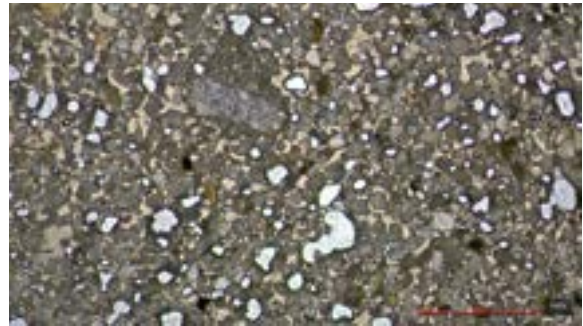

Fig.25a

Fig.25b

Fig.25c

Fig.25d

Fig. 25 Micrographs of samples of the outliers; a-b) the general composition of sample WM_11 (cross and plane polars, scale bar = 1 mm); c-d) the general composition of sample WM_22 (cross and plane polars, scale bar = 1 mm);

Table 6. Features and characteristics of samples analyzed by OM reorganized to petrographic groups

Group	Sample	Binder			Voids		Aggregate																		
		Type	Lumps amount	overall %	Types	overall %	carbonatic clasts	chert	quarts	sandstone	mica	clay pellets	feldspars	terracotta	chlorite	hematite	opaque minerals	Reused	Max grain size	Min grain size	Mean grain size	standrsd deviation	overall %	wentworth size class
1	WM_01	Calcic micritic	+ +	65	Vughs	5	+ + +	- -	-		- -	- -	- -				-		392.3	149.1	240.7	73.5	30	fine/medium
	WM_02	Calcic micritic	+ +	71	Vughs	5	+ + +	- -	-		- -		- -	- -		- -	-		229.9	124.2	175.0	29.4	24	fine
	WM_03	Calcic micritic	+ +	70	Vughs	9	+ + +	- -	-		- -		-	- -	-	- -	- -		433	173.7	281.8	61.9	21	medium
	WM_04	Calcic micritic	+ +	78	Vughs	7	+ + +	-	-		- -		-	-		- -	- -		385.2	167.5	265.3	62.3	15	medium
	WM_05	Calcic micritic	+	67	vughs, channels	8	+ + +	-	-		- -		- -	- -	- -	- -	- -		329.5	187.4	252.0	44.4	25	medium
	WM_06	Calcic micritic	+	67	Vughs	8	+ + +	- -	-			- -	-		- -	- -	- -		625.4	236.8	476.5	105.4	25	medium
	WM_07	Calcic micritic	+ +	63	Vughs	10	+ + +	- -	-		- -		-		- -	- -	- -		444.4	175.1	268.2	77.8	27	medium
	WM_08	Calcic micritic	+ +	62	Vughs	11	+ + +		+		- -		- -		- -	- -	- -		380.4	171.8	263.2	51.5	27	medium
	WM_09	Calcic micritic	+ +	64	Vughs	11	+ + +	-	-		- -	-	- -		- -		- -		391.8	151.2	270.9	60.6	25	medium
	WM_10	Calcic micritic	+	72	vughs, vesicles	10	+ + +	- -	-		- -		- -		- -	- -	- -		363.6	129.8	289.7	67.8	18	medium
	WM_12	Calcic micritic	+ +	70	Vughs	7	+ + +	- -	-		- -	- -	-			- -	- -		409.6	201.2	313.6	67.2	23	medium
	WM_13	Calcic micritic	+ +	73	vughs, vesicles	7	+ + +	- -	-				-		-	- -	-		337.6	181.2	275.7	57.6	20	medium
	WM_23	Calcic micritic	+ +	72	vughs, planar	5	+ + +	-	+		- -	- -	- -		- -	- -	- -		346.4	134.7	219.8	54.8	23	fine
	WM_24	Calcic micritic	+	70	Vesicles	6	+ + +	-	-		- -		- -			- -	- -		558.1	238	355.3	93.4	24	medium
	WM_25	Calcic micritic	+	80	Vughs	5	+	- -	-	- -	- -				- -	- -	- -		495.2	138.5	249.4	75.4	15	medium

| Group | Sample | Binder | | | Voids | | Aggregate | | | | | | | | | | | | | | | | | |
		Type	Lumps amount	overall %	Types	overal %	carbonatic clasts	chert	quarts	sandstone	mica	clay pellets	feldspars	terracotta	chlorite	hematite	opaque minerals	Reused	Max grain size	Min grain size	Mean grain size	standsrd deviation	overall %	wentworth size class
	WM_19	Calcic micritic	+	64	Vughs	7	+ + +		+				-		-	- -	- -		323.5	166.4	239.1	48.8	29	fine/medium
	WM_20	Calcic micritic	+	71	Vughs	5	+ + +	-	-		- -		-	- -	- -	- -			406.4	166.7	298.6	65.2	24	medium
2	WM_14	Calcic micritic	-	41	Vughs	6	+ +	-	-	+	- -	- -							7345	229	#####	#####	54	bivariate (fine sand and coarse sand)
	WM_16	Calcic micritic	- -	37	Vughs	9	+ +	-	-	+			- -				- -		5431	239	#####	#####	53	
	WM_17	Calcic micritic	- -	42	Vughs	3	+	-	- -	+	- -	- -			- -	- -	-		1841	141.4	529.4	388.4	55	bivariate (fine sand and coarse sand)
3	WM_26	Calcic micritic	-	44	Vughs, vesicles	11	+ + +	- -	-									+	374.5	139.2	258.8	68.2	45	medium
	WM_27	Calcic micritic	-	35	Vughs	15	+ +	+	-	-	- -	- -			-		- -	+	340.8	142.4	228.6	56.4	50	medium
Outlier_1	WM_11	Calcic micritic	+	43	Vughs	9	+ + +		+	-	- -		- -		- -	- -	- -		6824	181	698.5	#####	48	medium
Outlier_2	WM_22	Calcic micritic	- -	30	Vughs	19	+ + +	- -	-		- -		-			- -	- -		368.1	165.7	259.1	60.9	51	medium

s

6.4 SEM-EDS

For the SEM-EDS analysis, 6 samples from different groups were selected.
Group 1 - WM_9, group 2 - WM_16, WM_17, group 3 - WM_27 and outliers - WM_11, WM_22.

Group 1

Figure 26 represents the lump in the sample WM_9. The texture of the lump is typical for the carbonated lime as it has typical capillary pores. The chemical composition of the lump is shown in figure 18 and calcium (Ca) is defined to be the main element. A small amount of magnesium (Mg), silicon (Si) and chlorine (Cl) is present as well.
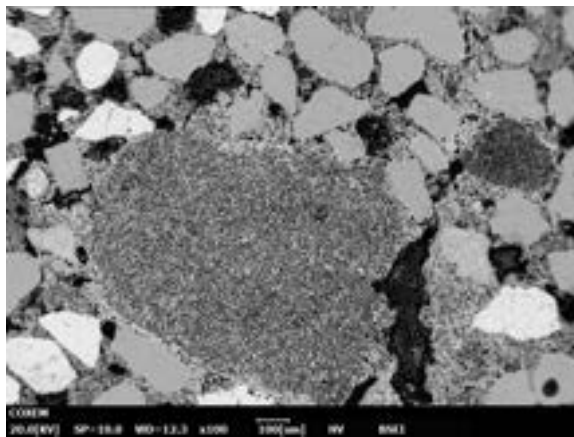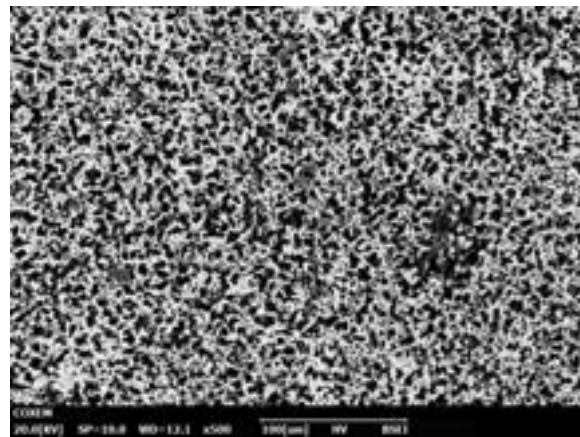
| Fig.26a | Fig.26b |

Fig. 26 SEM-EDS images of a lime lump in the sample WM_9; a) magnification 100x, b) magnification 500x
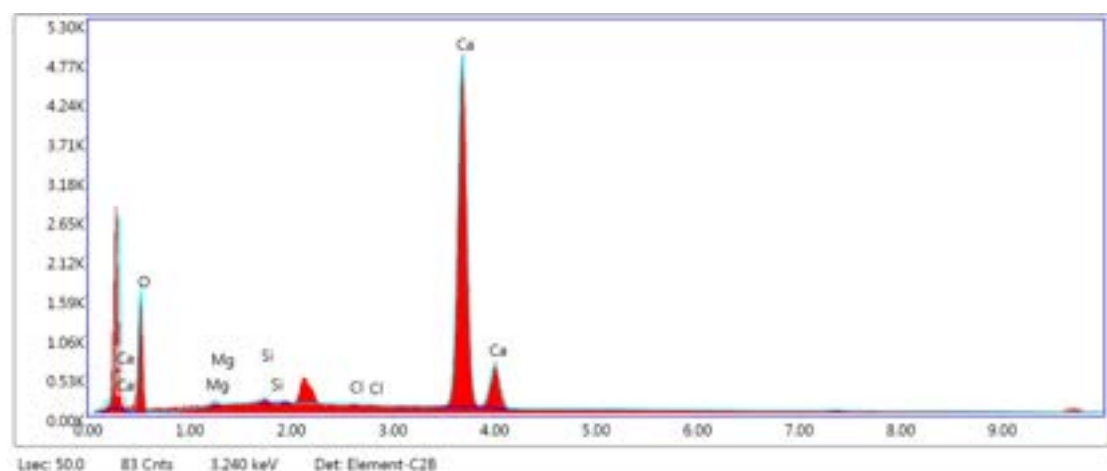
Fig. 27 Chemical composition of the lump WM_9

The aggregates exhibit clean and well-defined edges, with no reaction rims observed (Fig.28), indicating no interaction between the aggregates and the binder. The lime is adequately calcined, and there are no remnants of incomplete calcination, which means that the lumps are

present due to poor mixing. The chemical composition of the binding matrix consists mainly of calcium (Fig.29). Low amount of silicon indicates that there was no pozzolanic reaction.
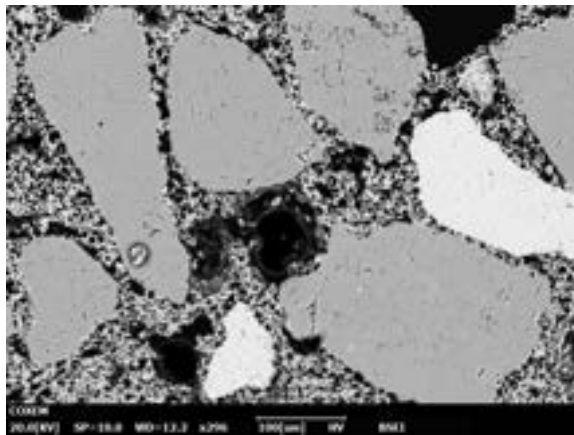
Fig.28a
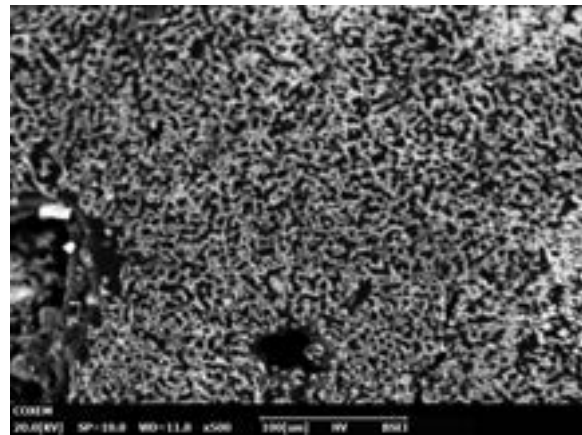
Fig.28b

Fig. 28 SEM-EDS image of a binding matrix and aggregates of the sample WM_9; a) magnification 100x, b) magnification 500x
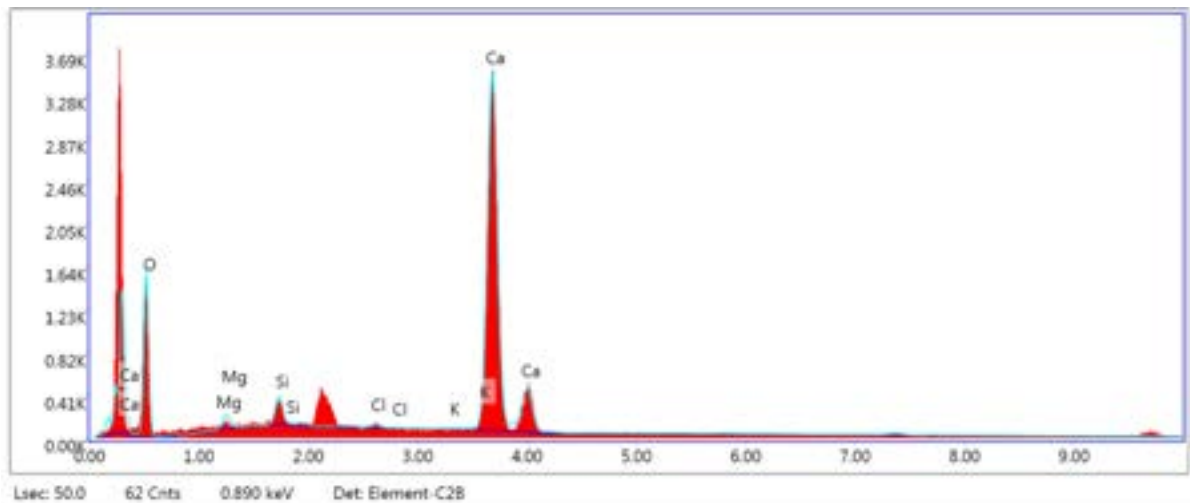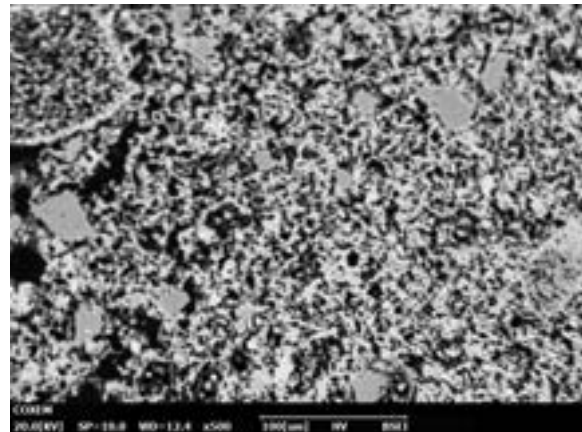

Fig. 29 Chemical composition of the binding matrix WM_9

Group 2

Figure 21 represents the binding matrix and aggregates of the sample WM_16. This sample is characterized by the absence of lime lumps and a big amount of aggregates. The aggregates display clean, well-defined edges with no reaction rims observed (Fig. 30), suggesting no interaction between the aggregates and the binder. The lime is properly calcined, with no remnants of incomplete calcination. The binding matrix is primarily composed of calcium (Fig. 31). The low silicon content indicates the absence of a pozzolanic reaction.
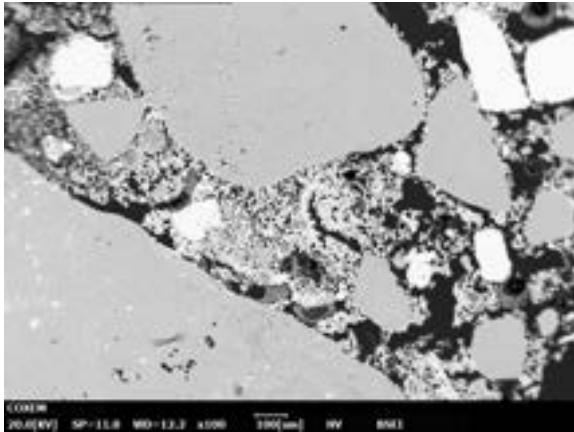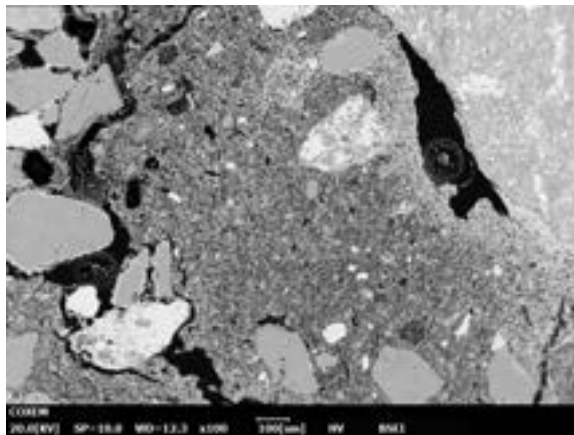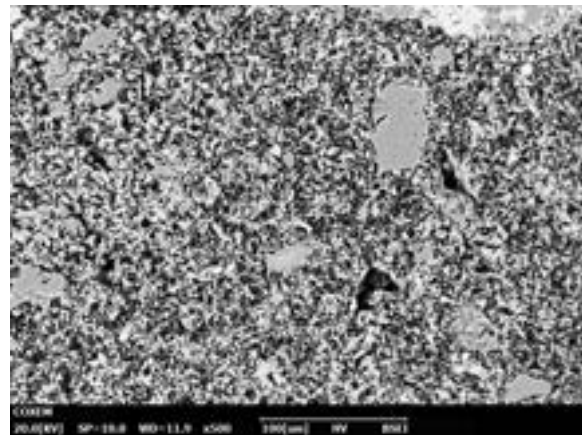
Fig.30a
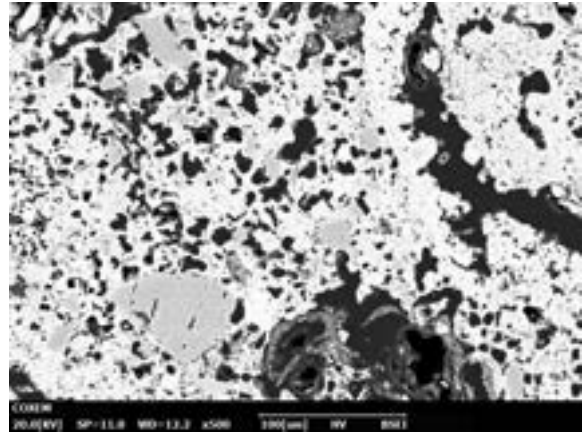
Fig.30b
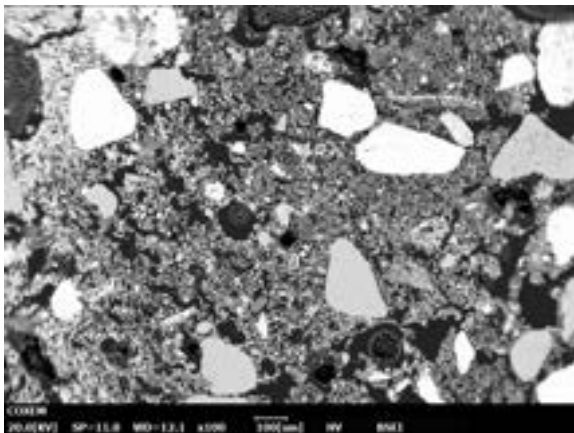
Fig.30c
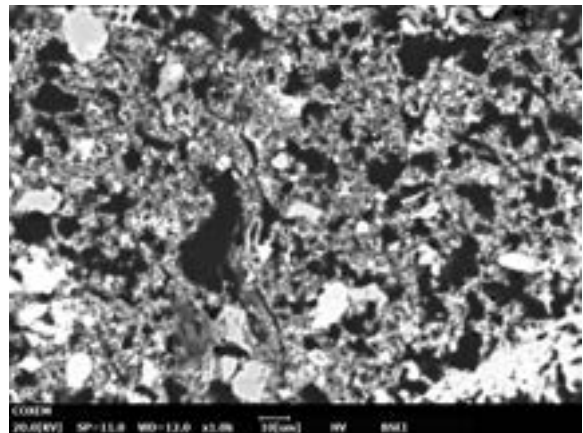
Fig.30d

Fig. 30 SEM-EDS image of different points of a binding matrix and aggregates of the sample WM_16; a) magnification 100x, b) magnification 500x, c) magnification 100x, d) magnification 1000x
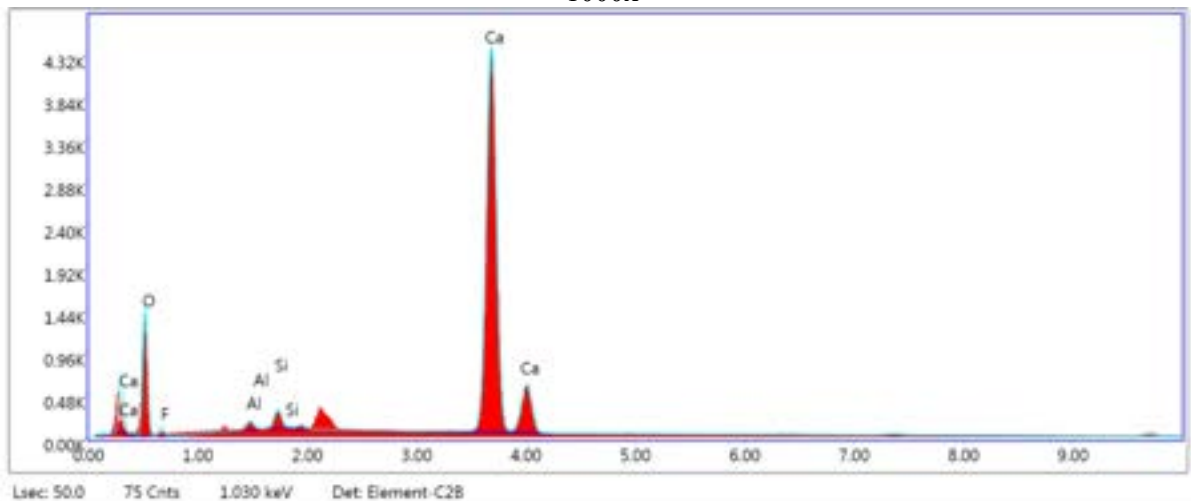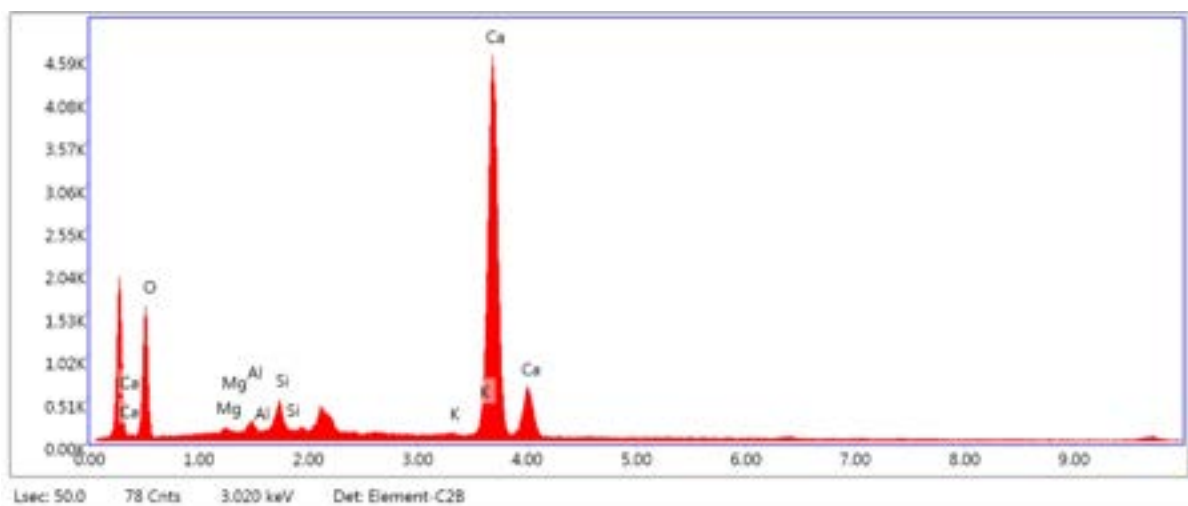

Fig. 31 Chemical composition of the binding matrix of the sample WM_16

Figure 23 illustrates the binding matrix and aggregates of sample WM_17, which is notable for the absence of lime lumps. The aggregates exhibit clean, well-defined edges without reaction rims (Fig. 32), indicating no interaction between the aggregates and the binder. The lime is properly calcined, with no remnants of incomplete calcination. The binding matrix primarily

60

consists of calcium (Fig. 33), and the low silicon content suggests the absence of a pozzolanic reaction.
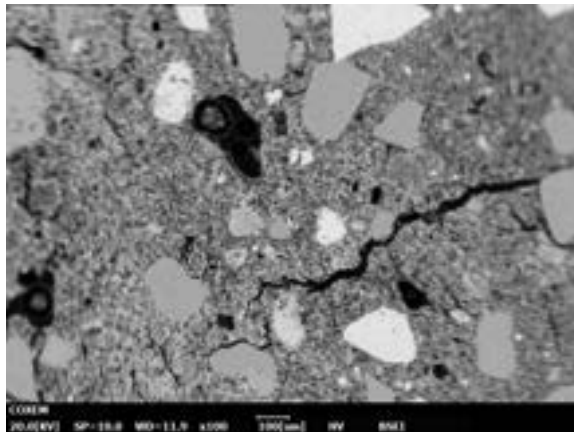
Fig.32a

Fig.32b

Fig.32c

Fig.32d

Fig. 32 SEM-EDS image of different points of a binding matrix and aggregates of the sample WM_17; a) magnification 100x, b) magnification 500x, c) magnification 100x, d) magnification 500x

Fig. 33 Chemical composition of the binding matrix of the sample WM_17

Group 3

WM_27

Figure 34 depicts the lump in sample WM_27. The texture of the lump, characterized by typical capillary pores, is indicative of carbonated lime. The chemical composition of the lump, shown in Figure 35, identifies calcium (Ca) as the predominant element, with small amounts of magnesium (Mg), silicon (Si), and chlorine (Cl) also present.
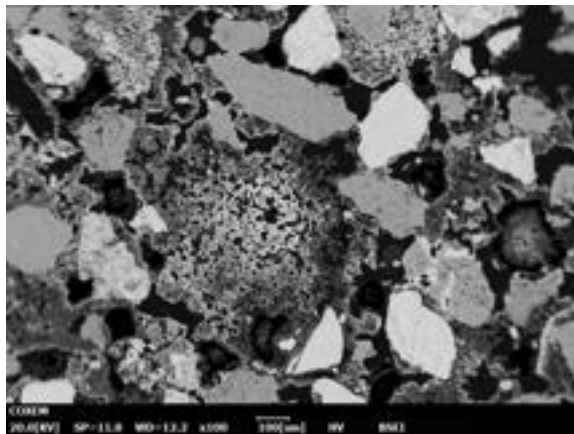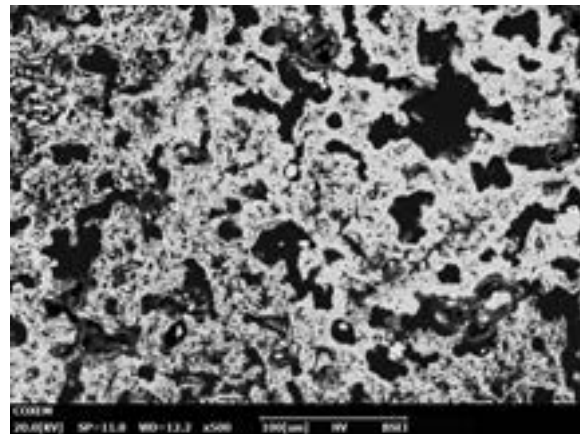
Fig.34a   Fig.34b

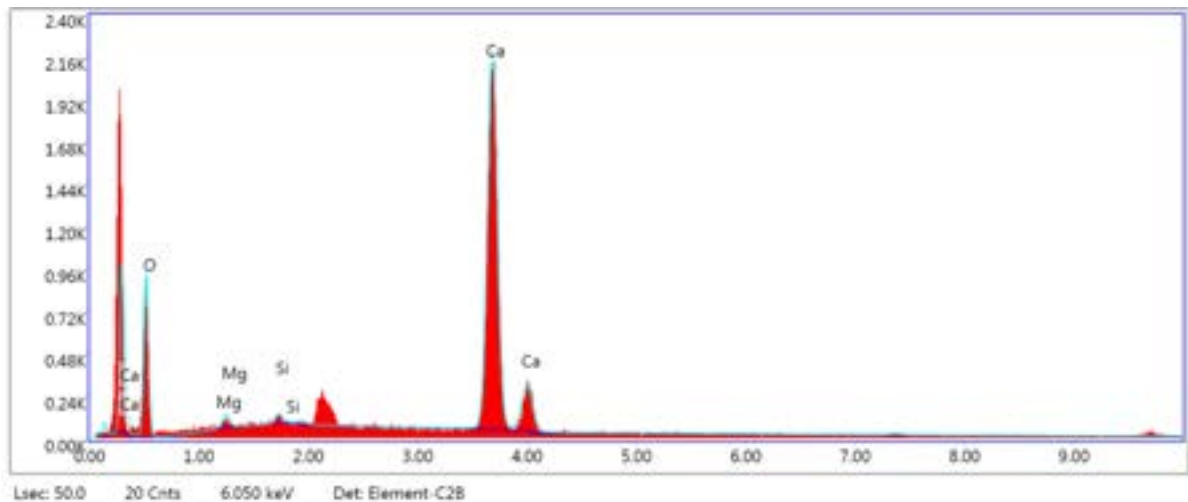Fig. 34 SEM-EDS images of a lime lump in the sample WM_27; a) magnification 100x, b) magnification 500x

Fig. 35 Chemical composition of the lime lump WM_27

The numerous aggregates display clean, well-defined edges with no reaction rims observed (Fig. 36), indicating no interaction between the aggregates and the binder. The lime is properly calcined, with no remnants of incomplete calcination, suggesting that the lumps are present due to poor mixing. The binding matrix is primarily composed of calcium (Fig. 37), and the low silicon content indicates the absence of a pozzolanic reaction.

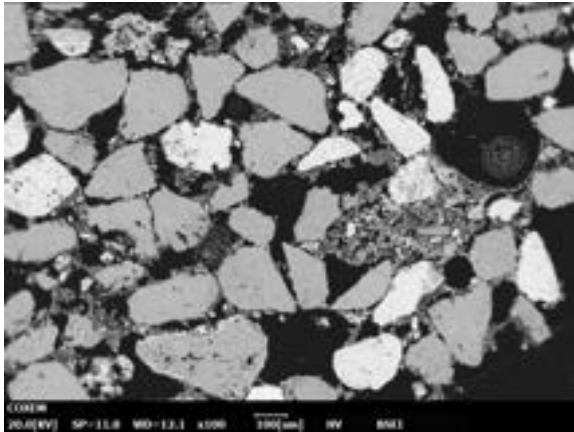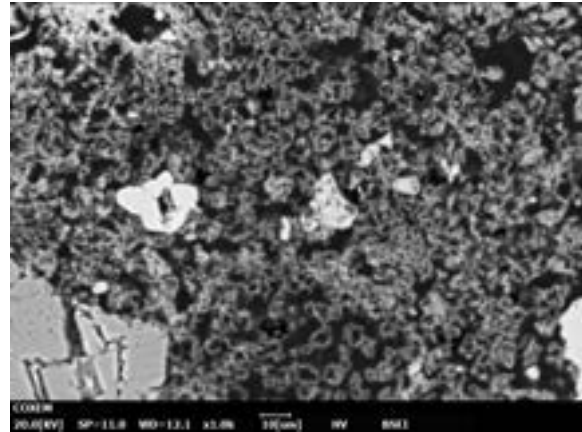<div align="center">Fig.36a   Fig.36b</div>

Fig. 36 SEM-EDS image of a binding matrix and aggregates of the sample WM_27; a) magnification 100x, b) magnification 1000x
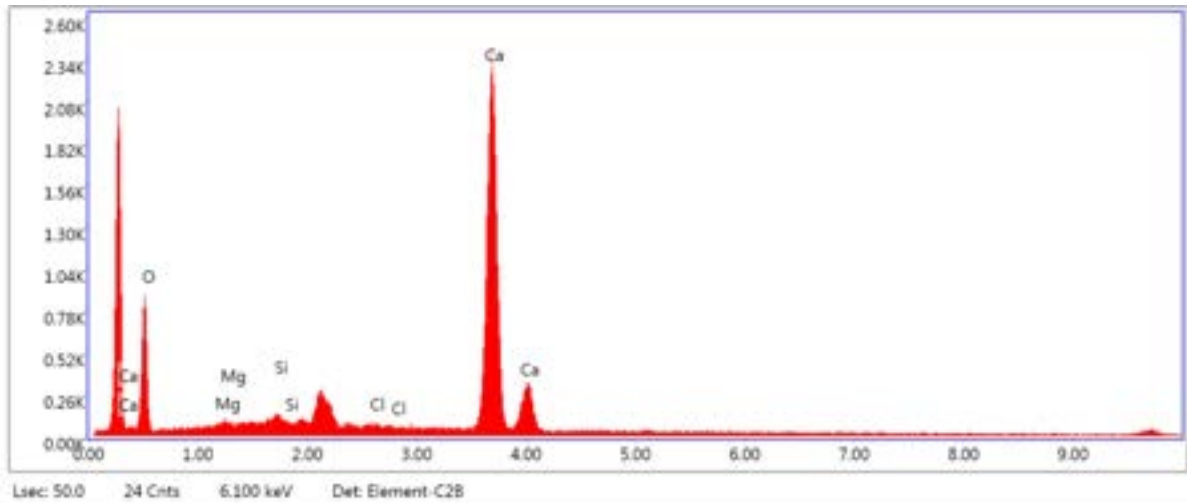

Fig. 37 Chemical composition of the binding matrix sample WM_27

Outliers

Sample WM_11 exhibits a calcination relict (Fig. 38), indicating incomplete conversion of the lime binder during the calcination process. The relict primarily consists of calcium, with a minor presence of silicon, likely attributable to impurities or inadvertent inclusion (Fig. 39).
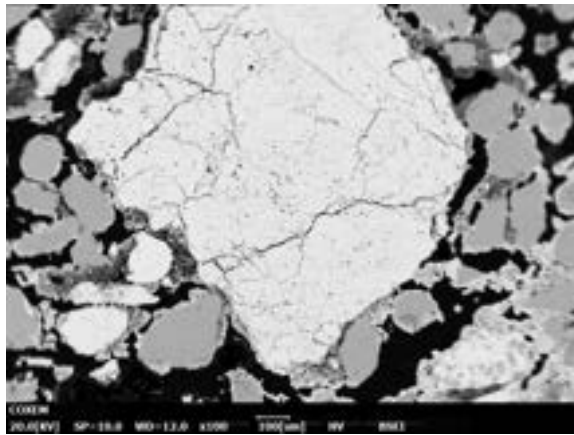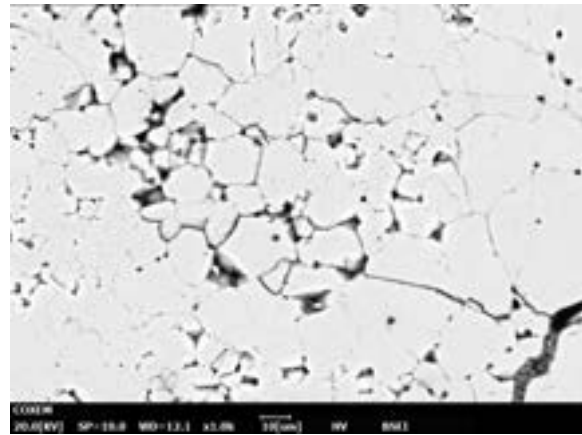

Fig.38a   Fig.38b

Fig. 38 SEM-EDS image of a calcination relict in the sample WM_11; a) magnification 100x, b) magnification 1000x
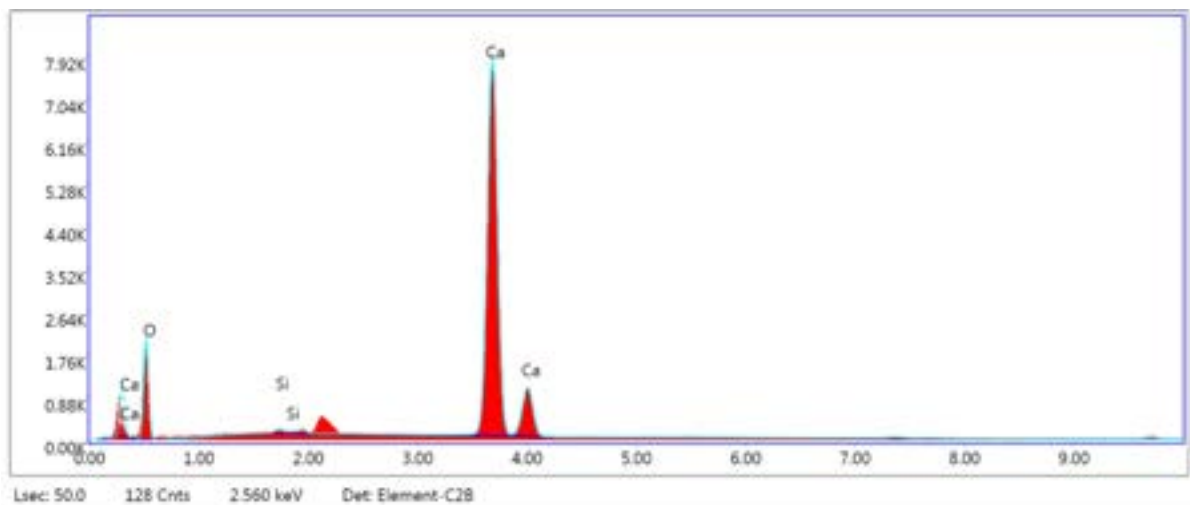

Fig. 39 Chemical composition calcination relict WM_11

The aggregates are present with clean, well-defined edges. No reaction rims are observed (Fig. 40), indicating no interaction between the aggregates and the binder. The binding matrix is primarily composed of calcium (Fig. 41) as well as minor presence of magnesium, aluminum and silicon. The low silicon content indicates the absence of a pozzolanic reaction.
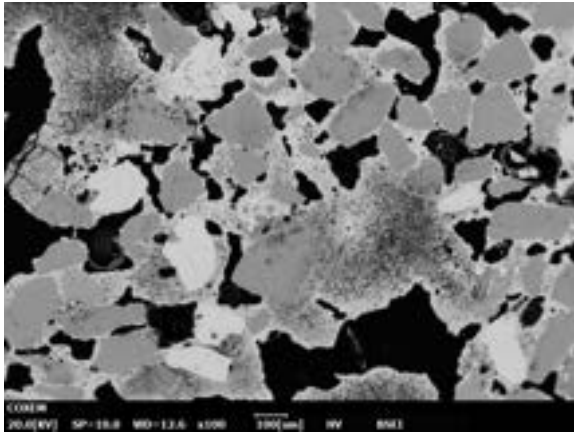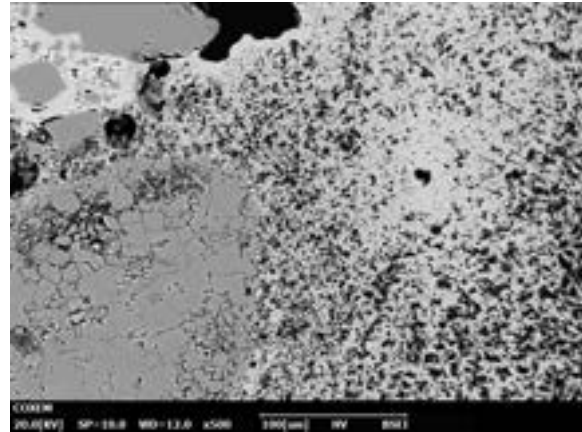
<div align="center">Fig.40a   Fig.40b</div>

Fig. 40 SEM-EDS image of a binding matrix and aggregates of the sample WM_1; a) magnification 100x, b) magnification 500x
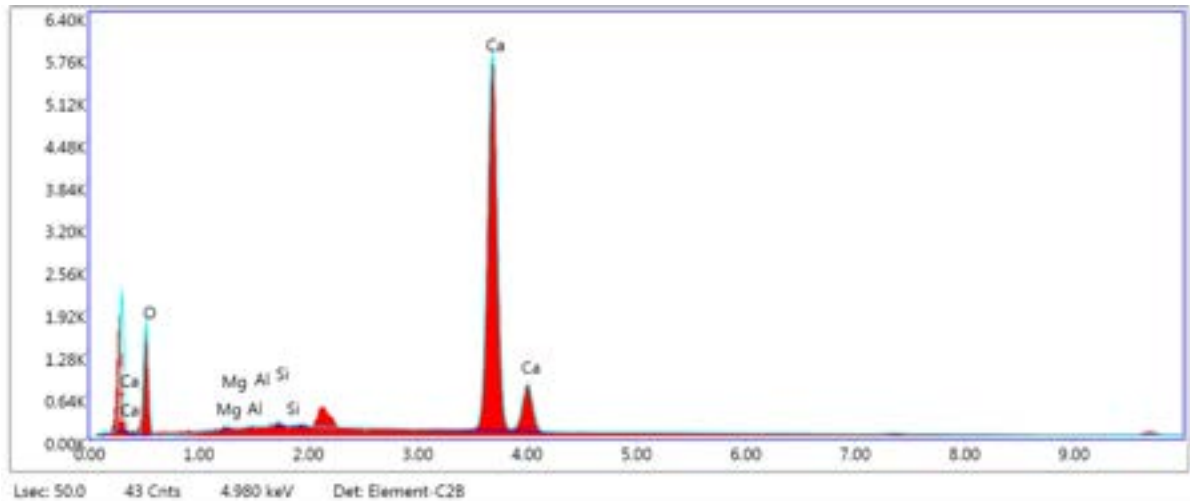

Fig. 41 Chemical composition of the binder WM_11

Figure 42 represents the binding matrix and aggregates of the sample WM_22. This sample is characterized by the absence of lime lumps and a big amount of aggregates. It can be characterized as a lean mortar. The aggregates display clean, well-defined edges with no reaction rims observed (Fig.42a,c), suggesting no interaction between the aggregates and the binder. The lime is properly calcined, with no remnants of incomplete calcination. The binding matrix is primarily composed of calcium (Fig. 43). The low silicon content indicates the absence of a pozzolanic reaction.
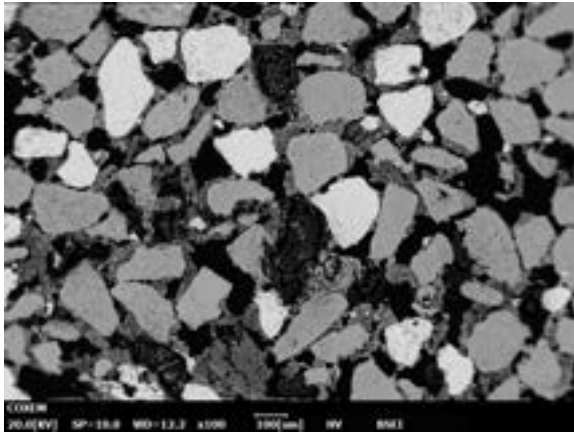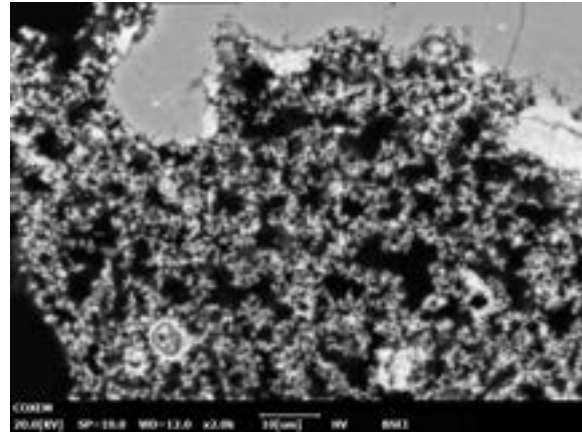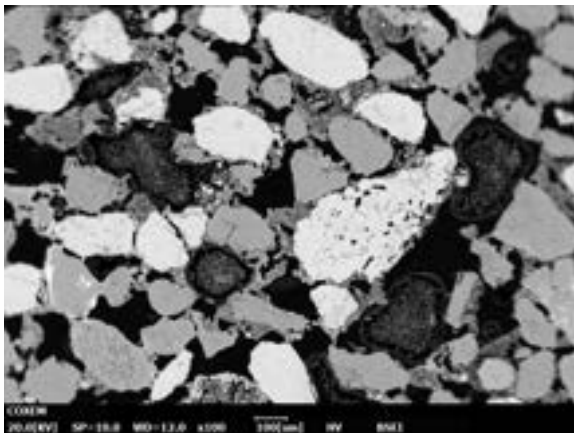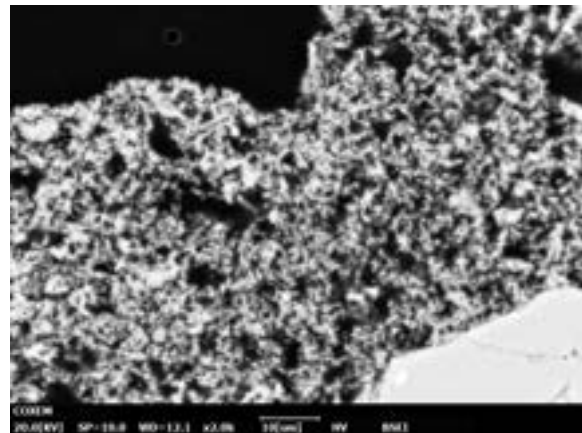
Fig.42a

Fig.42b

Fig.42c

Fig.42d

Fig. 42 SEM-EDS image of different points of a binding matrix and aggregates of the sample WM_22; a) magnification 100x, b) magnification 2000x, c) magnification 100x, d) magnification 2000x
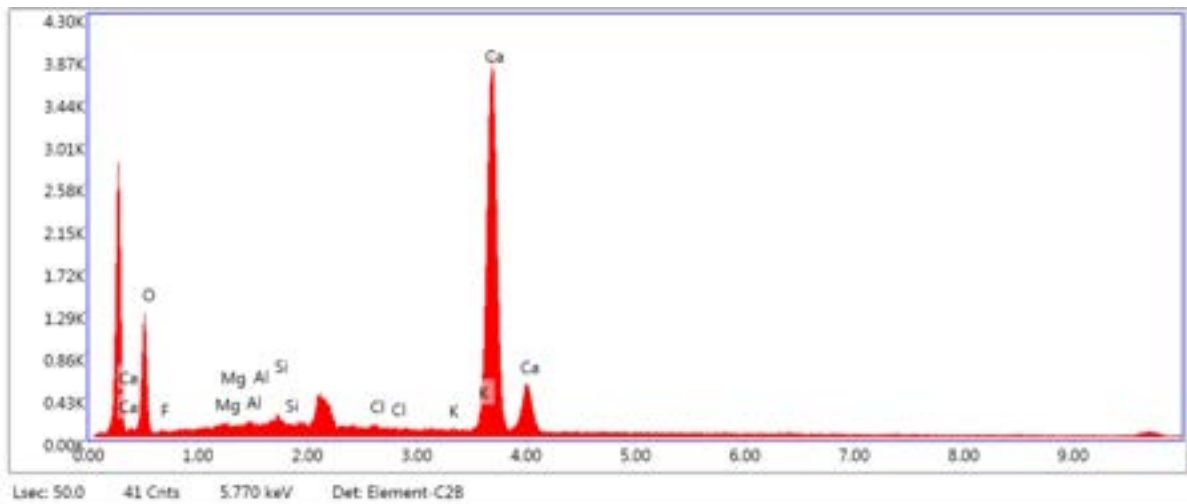

Fig. 43 Chemical composition of the binding matrix WM_22

Hydraulic index

According to the study of Pecchioni, Fratini and Cantisani (2008), the hydraulic index ranges from 0 to 1.2. A value of zero indicates the absence of hydraulic properties, signifying aerial lime. An index of 0.5 suggests the material is either weak lime or cement, whereas values up to 1.2 denote rapid-setting cements.

WM_16

Table 7. eZAF Smart Quant Results with Oxides of the sample WM_16

Element	Weight %	Atomic %	Net Int.	Error %	Kratio	Z	A	F
F 2O	6.50	6.80	12.11	17.33	0.0040	1.0197	0.0913	1.0000
Al 2O3	1.57	0.87	13.27	17.94	0.0039	0.9794	0.5085	1.0046
Si O2	3.39	3.19	33.37	12.13	0.0096	1.0015	0.6419	1.0073
Ca O	88.54	89.14	974.08	1.64	0.5588	0.9482	0.9985	1.0014

$HI(Al_2O_3 + Fe_2O_3 + SiO_2)/(CaO+MgO) = 0.129$

The HI is close to 1.2, which corresponds to the upper limit for quick-setting lime. The mortar can be characterized as aerial.

WM_17

Table 8. eZAF Smart Quant Results with Oxides of the sample WM_17

Element	Weight %	Atomic %	Net Int.	Error %	Kratio	Z	A	F
Mg O	0.61	0.85	4.35	52.81	0.0013	1.0184	0.3698	1.0026
Al 2O3	1.46	0.81	12.57	19.85	0.0036	0.9814	0.5159	1.0047
Si O2	5.07	4.78	50.77	9.51	0.0143	1.0037	0.6491	1.0073
K 2O	0.23	0.14	3.68	62.28	0.0017	0.9330	0.9767	1.0696
Ca O	92.63	93.43	1021.95	1.72	0.5745	0.9505	0.9956	1.0012

$HI(Al_2O_3 + Fe_2O_3 + SiO_2)/(CaO+MgO) = 0.07$

The HI is lower than 1.2, which corresponds to the upper limit for quick-setting lime. The mortar can be characterized as aerial.

WM_11

Table 9. eZAF Smart Quant Results with Oxides of the sample WM_11

Element	Weight %	Atomic %	Net Int.	Error %	Kratio	Z	A	F
Mg O	0.73	1.01	6.00	38.37	0.0015	1.0215	0.3631	1.0025
Al 2O3	0.11	0.06	1.12	79.61	0.0003	0.9845	0.5076	1.0046
Si O2	0.81	0.75	9.48	25.50	0.0023	1.0068	0.6478	1.0077
Ca O	98.35	98.17	1280.84	1.60	0.6273	0.9536	1.0028	1.0011

HI(Al_2O_3 + Fe_2O_3 + SiO_2)/(CaO+MgO) = 0.009

The HI is lower than 1.2, which corresponds to the upper limit for quick-setting lime. The mortar can be characterized as aerial.

Aerial lime typically exhibits properties such as high permeability, flexibility, and plasticity. It tends to shrink during the early stages of hardening, is soluble in water, and has relatively low mechanical strength [29].

6.5 Digital image analysis (DIA)

The digital image analysis results allowed the creation of a ternary plot (Fig.44). It illustrates the compositional distribution of samples in terms of three components: aggregate, binder, and porosity percentage. Each point on the plot represents a specific composition of these three components for a sample, with the percentages summing to 100% at any given point.

The bottom axis of the plot represents the binder percentage, ranging from 25% to 75%, indicating the proportion of binder in the samples. The left axis corresponds to the aggregate percentage, which spans from 0% to 75%, denoting the proportion of aggregate. The right axis, representing the porosity percentage, ranges from 0% to 50%, indicating the level of porosity within the samples.

The plot categorizes the samples into different groups. Group 1 (Gr 1), represented by the green color, predominantly occupies the region with high binder percentages and low aggregate and porosity percentages. Group 2 (Gr 2), depicted by pink circles, is distributed across the middle range of binder percentages, with relatively higher aggregate and porosity percentages compared to Gr 1. Group 3 (Gr 3), shown as gray circles, is scattered mostly in the middle of the plot, indicating a balanced mix of aggregate, binder, and porosity percentages.

The plot also identifies outliers, distinguished by the red and orange color. Sample WM_11 (outlier 1) marked by red circles, has a distinct composition, possibly due to higher porosity or different aggregate and binder ratio. Sample WM_22 (outlier 2), marked by an orange circle, also has a unique composition, differing from Outlier 1 and the main groups, potentially due to higher aggregate or binder content.

Sample WM_27 from Gr 3, located centrally on the plot, suggests a balanced composition of aggregate, binder, and porosity percentages. Similarly, WM_26 from Gr 3, positioned close to the binder percentage axis, indicates a higher binder content with moderate porosity and aggregate. Samples WM_16 and WM_17 from Gr 2, situated near each other, reflect similar compositions with moderate binder and higher aggregate and porosity content.
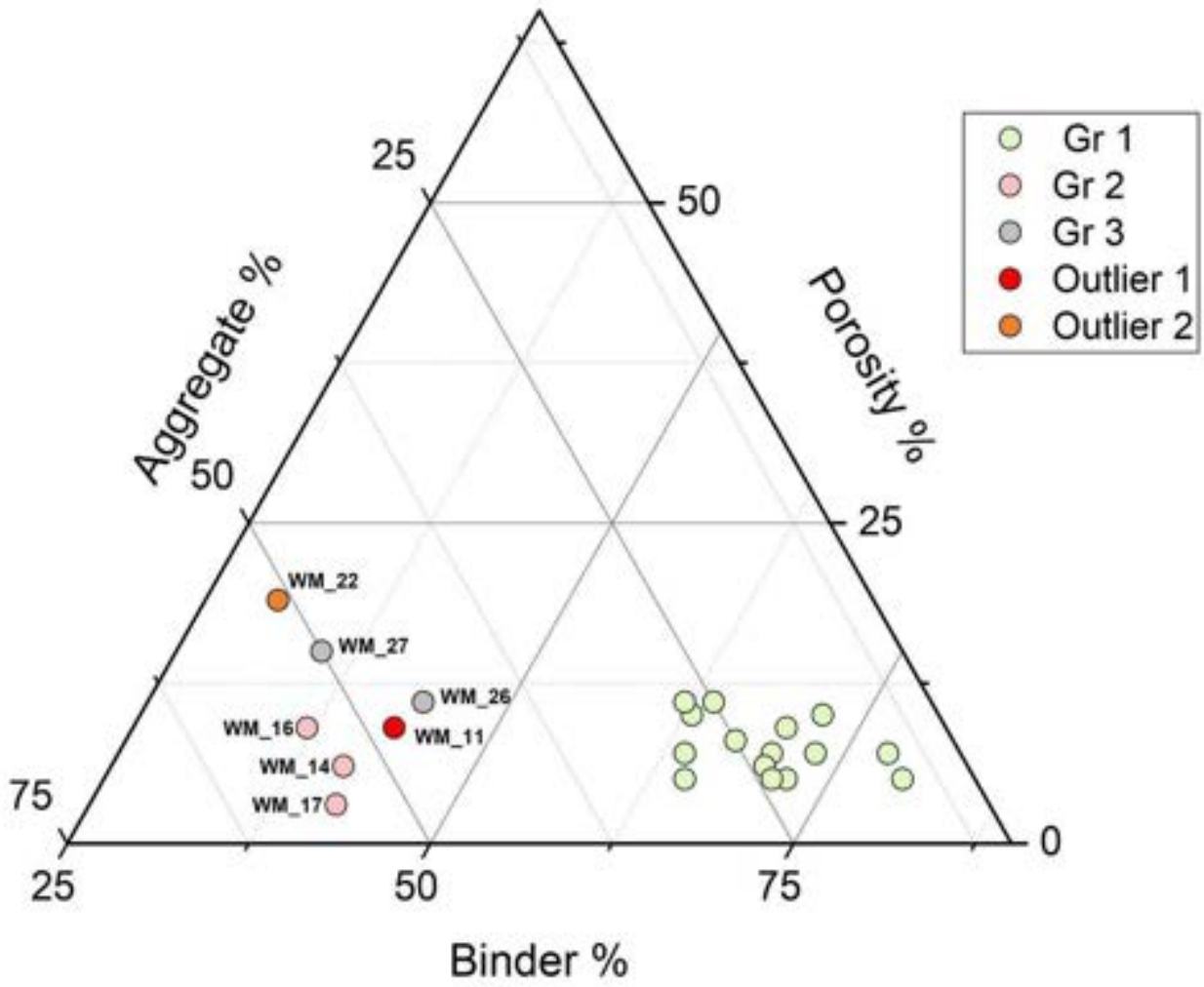
Fig. 44 Ternary plot diagram for the analyzed wall mortars, reporting the % of binder, aggregate and porosity rates calculated after DIA analyses of thin sections scans.

Chapter 7. Discussion

Following the chemical and mineralogical analyses of the samples from the Roman Villa of Mutteron dei Frati in Bibione, we have obtained substantial information regarding the composition of the mortars used in the construction of the villa's walls.

The absence of significant pozzolanic reactions in all samples suggests the use of freshwater rather than saline water in the mixing process, as the latter would typically induce the formation of pozzolanic phases [30]. XRPD analysis has revealed a heterogeneous composition of the aggregates, comprising both silicate and carbonate clasts, nonetheless the samples from the northern part of the villa have differences in mineral composition from the samples from the southern part. Optical microscopy analysis further confirmed that the aggregate grain size ranges from fine to medium sands. This observation is consistent with the local geology, particularly the proximity of coastal dunes, which likely provided the sand used in the construction materials.

Moderate amount of pores in all the samples studied by OM indicates a rather well-balanced mix that achieves good workability, adequate strength and durability of the mortar.

The presence of chert, identified through OM, indicates that the materials have undergone physical weathering and subsequent transport prior to their deposition in the current sedimentary context. This is corroborated by the identification of fine chert particles within the sediment, which suggests wind transportation as a significant contributing process. Such aeolian processes are characteristic of arid environments, where fine chert particles can be entrained and deposited as part of aeolian sediments, including loess or dune deposits.

These findings imply that the construction materials exhibit a complex history of weathering and transport, reflecting both fluvial and aeolian influences. The geological setting, characterized by nearby coastal dunes, further supports the hypothesis of local sourcing and reworking of the sand aggregates, underscoring the interplay between physical weathering, wind transportation, and sediment deposition in the formation of the observed material composition.

Group 1 (WM_01, WM_02, WM_03, WM_04, WM_05, WM_06, WM_07, WM_08, WM_09, WM_10, WM_12, WM_13, WM_19, WM_20, WM_23, WM_24, WM_25), defined by petrographic analysis, has similar characteristics visible in optical microscope and quite similar mineralogical composition. It is also confirmed by the digital image analysis as this group falls into the region with high binder percentages and low aggregate and porosity percentages. Their colorimetric parameters coincide as well, which is proved by the colorimetric analysis and further statistical treatment.

It is thus possible to suggest that the samples of Group 1 belong to an older construction phase. The phase was rather consistent as there are no significant differences in the composition of

the mortar. The presence of lumps in the samples can be attributed to the poor mixing rather than to unproper calcination of the limestone used for binder production. The samples of this group also do not contain any reused mortar particles.

The samples WM_10 and WM_25, however, can be described as slightly fatter mortars, but it is likely that this was not an intentional accidental variation.

As the Fig. 45 depicts, the highlighted part of the structure has a different orientation of the walls. There was a hypothesis that the walls of this part of the building were built during a later construction phase. However, the results of the analysis of this research disprove this hypothesis as the various samples taken from different walls demonstrate similar composition and texture. So, the new suggested hypothesis is that the parts were built in one construction phase, or there were two phases, but the same kind of materials were used.

However, there is one outlier which is located at the same area, identifiable in sample WM_11. According to the optical microscopy analysis, it contains a calcination relict, which makes this sample unique out of the set. It primarily consists of medium grain size aggregates, nevertheless it contains some coarse ones. It is also located in a lower stratigraphic layer US 6 (Fig.46). Given all these evidence, it is possible to suggest that the sample WM_11 likely belongs to an older structure, related to a previous construction phase.
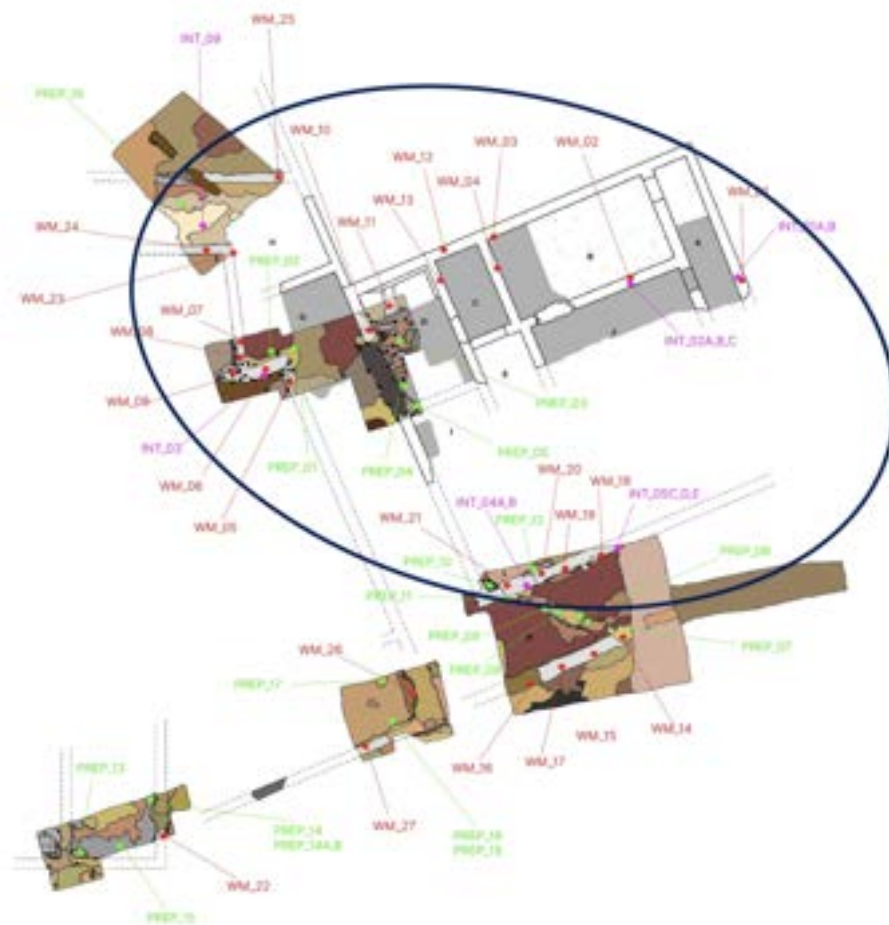

Fig. 45 Sampling points, group 1

Fig. 46 Sample WM_11, stratigraphic position

Group 2 (WM_14, WM_16, WM_17), defined by the similar characteristics in petrography, clusters leaner mortars with a bigger amount of aggregates and pores. The aggregates were defined as bivariate - fine and coarse sand, which can be a sign of the fact that a different or several various sources of sand was used in this construction phase. Fine gravels are present in the aggregates, and lime lumps are absent. The separation of this group was also confirmed by the digital image analysis. According to their position (Fig.47), the three samples come from the same southern wall. Due to the slightly different composition and porosity of the samples, it may be suggested that these samples belong to another construction phase, most likely a later one. Another hypothesis is that this part was an open porch at first, which was later closed and turned into a wall.
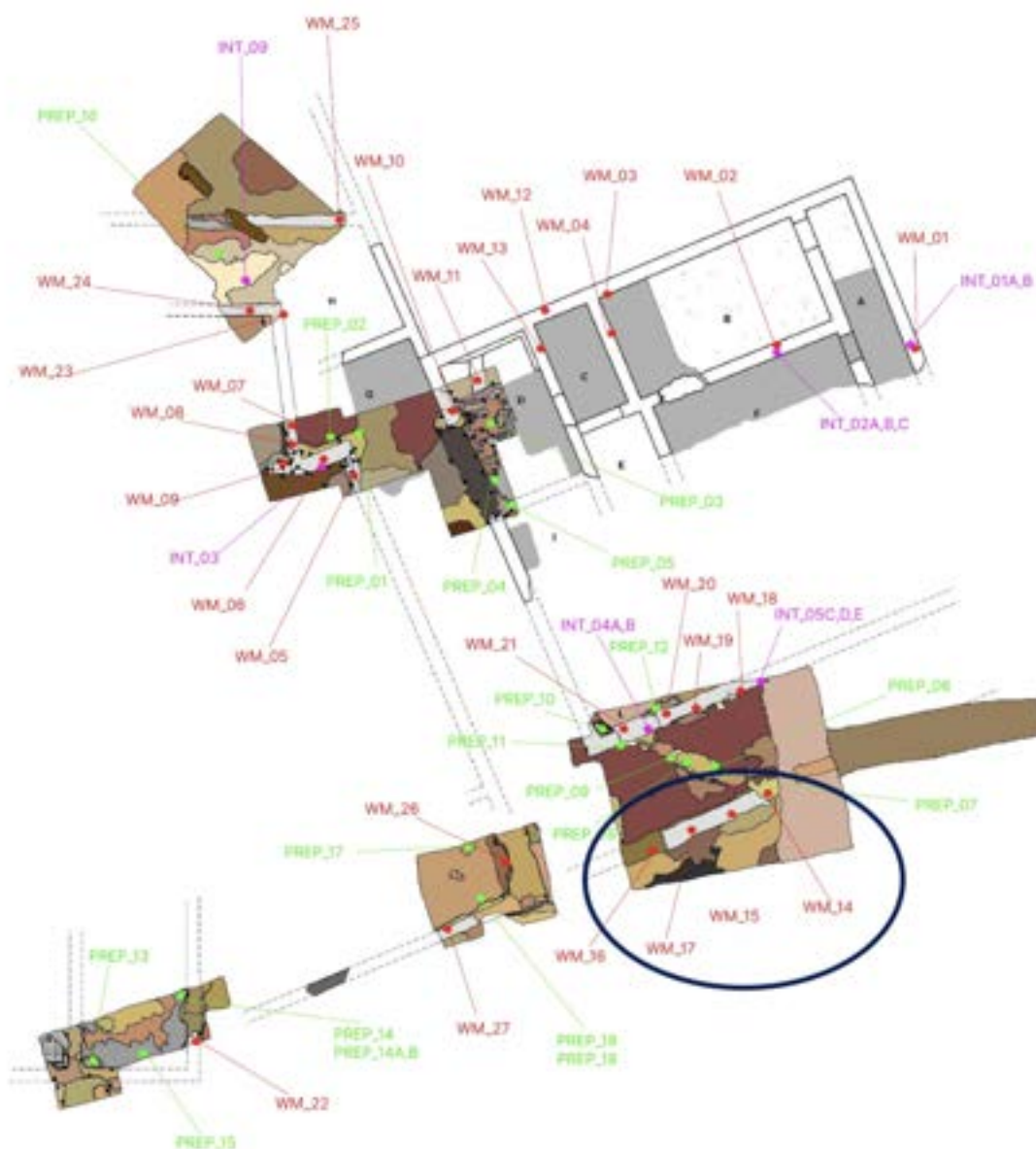
Fig. 47 Sampling points, group 2

Group 3 (WM_26, WM_27) is located in the south-west part of the excavation area (Fig.48). The main characteristic of these samples is the presence of pieces of reused mortar, as no other samples possess this peculiarity. The amorphous phase of these samples has the lowest values as it was reported in table 4. The aggregates belong to a medium sands grain size, suggesting that the sand source was the same as the one used for the samples in the Group 1. According to PCA data of XRPD analysis, these samples are slightly richer in dolomite. The results of the colorimetric analysis also put them in one group. Given all the facts, the hypothesis may be that this part of the villa was either built during a later construction phase with respect to the first one, or the walls were restored during the Late Antiquity period.
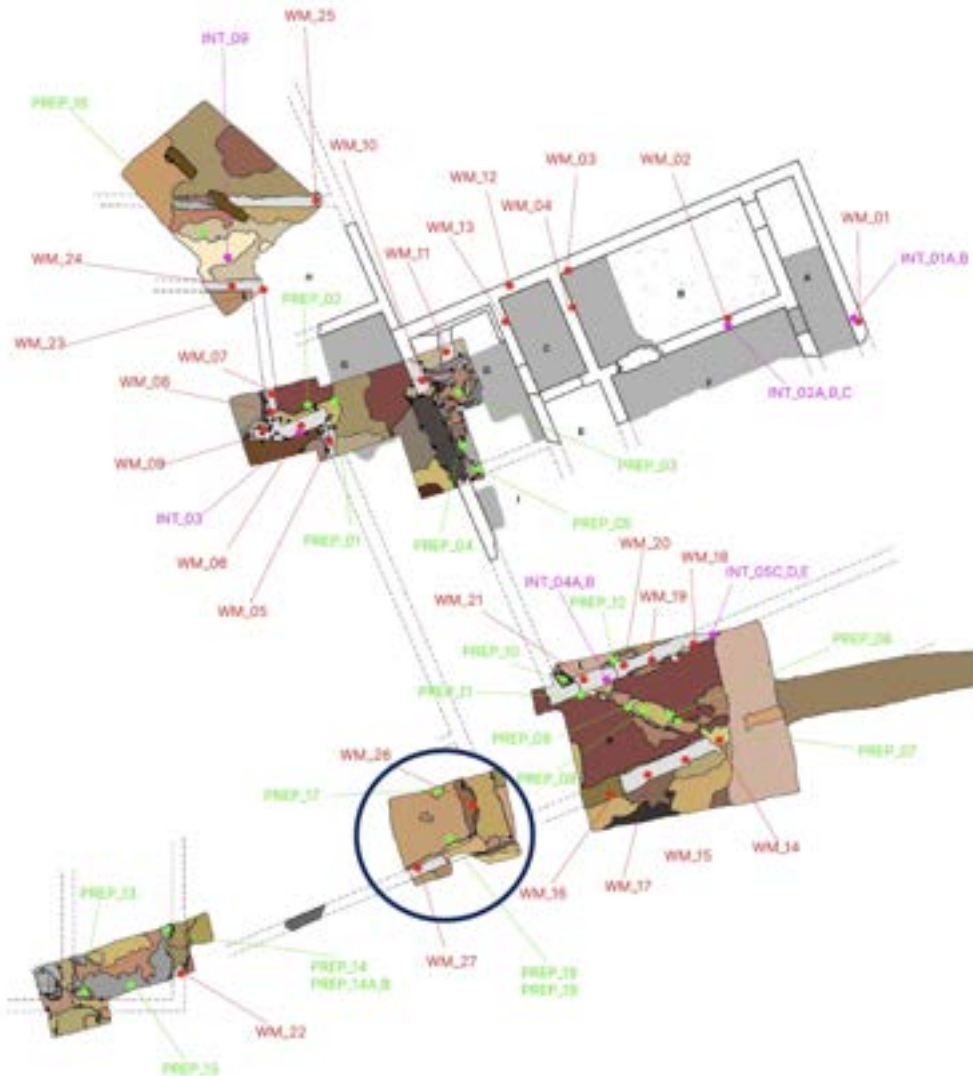
Fig. 48 Sampling points, group 3

The sample WM_22 is considered another outlier and it is located in the most western part of the villa (Fig.49). The optical microscopy analysis revealed the absence of lumps and a leaner mortar composition, which distinguishes this sample from the Group 3, for example, given their rather close proximity to each other. This sample is also rich in dolomite, and it has the highest porosity out of all the studied samples. The orientation of the walls according to the plan also differs from the rest of the structure, and the position of this sample was lower than the sample PREP_14, which was a preparatory layer for a floor mosaic (Fig.50). This fact can support the hypothesis that this part belongs to an older construction phase. Another hypothesis might appear as the orientations of the walls of the samples WM_11 and WM_22 are more alike rather than, for example, the wall of the sample WM_26 or WM_05, so it may be suggested that these two outliers actually belong to one previous construction phase. They may have been parts of one building or two separate ones. Their composition is not significantly different, but the percentage of voids or mean grain size of aggregate varies.
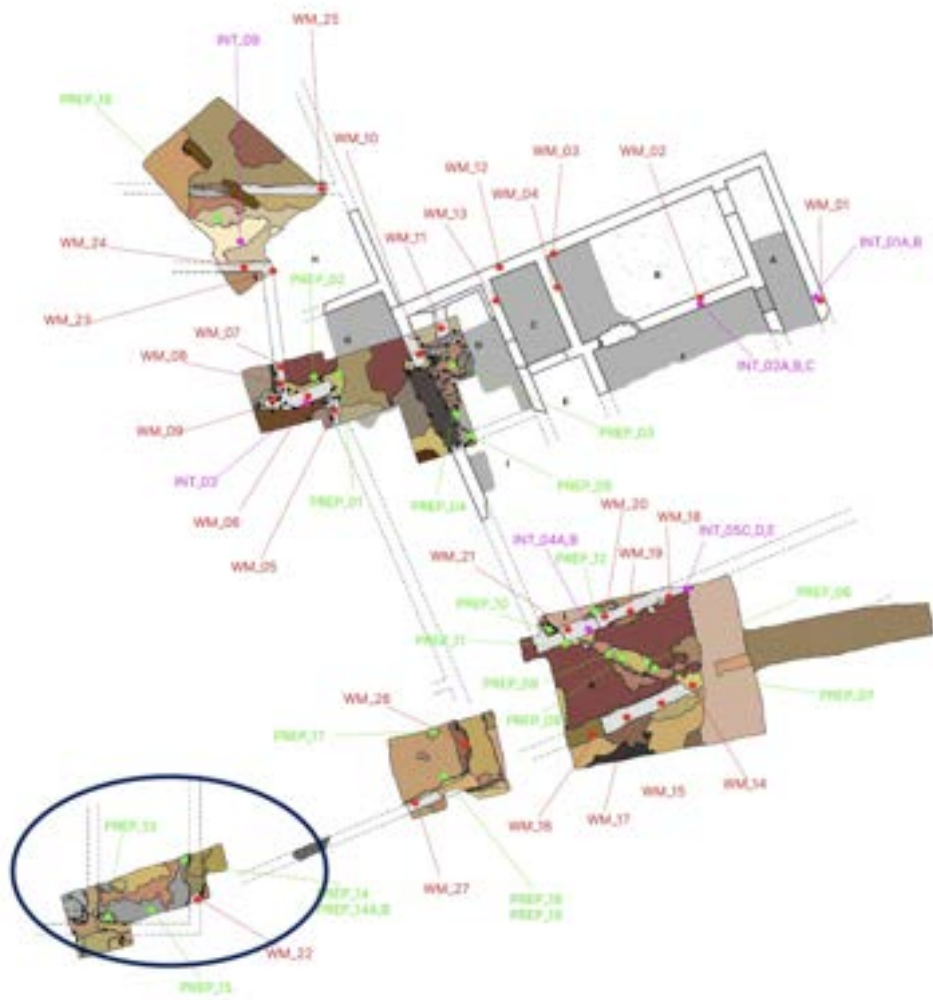
Fig. 49 Sampling point, outlier WM_22

<table>
<tr><td>Fig.50a</td><td>Fig.50b</td></tr>
</table>

Fig. 50 Sample WM_22, stratigraphic position

The analysis of preparatory layers confirms the differentiation of construction phases as the samples from Group 1 do not possess any presence of cocciopesto. Sample PREP_07 and PREP_09, however, are described as cocciopesto floors (high amorphous content, reddish hue in colorimetric analysis, presence of terracotta pieces and they are located in the south-eastern part of the villa, proving the different techniques. The sample WM_2 from the Group 1, nevertheless, is also described as a cocciopesto floor, which may imply restoration.

Thus, it is possible to hypothesize that the villa underwent three distinct construction phases and a subsequent restoration. Figure 51 illustrates the potential attribution of the areas and phases. The earliest phase, located at the lowest stratigraphic level, is highlighted in yellow. The primary phase, encompassing the majority of the villa, is depicted in dark blue. The green circle denotes the phase during which the open porch was likely enclosed. The light blue color corresponds to the wall restoration.
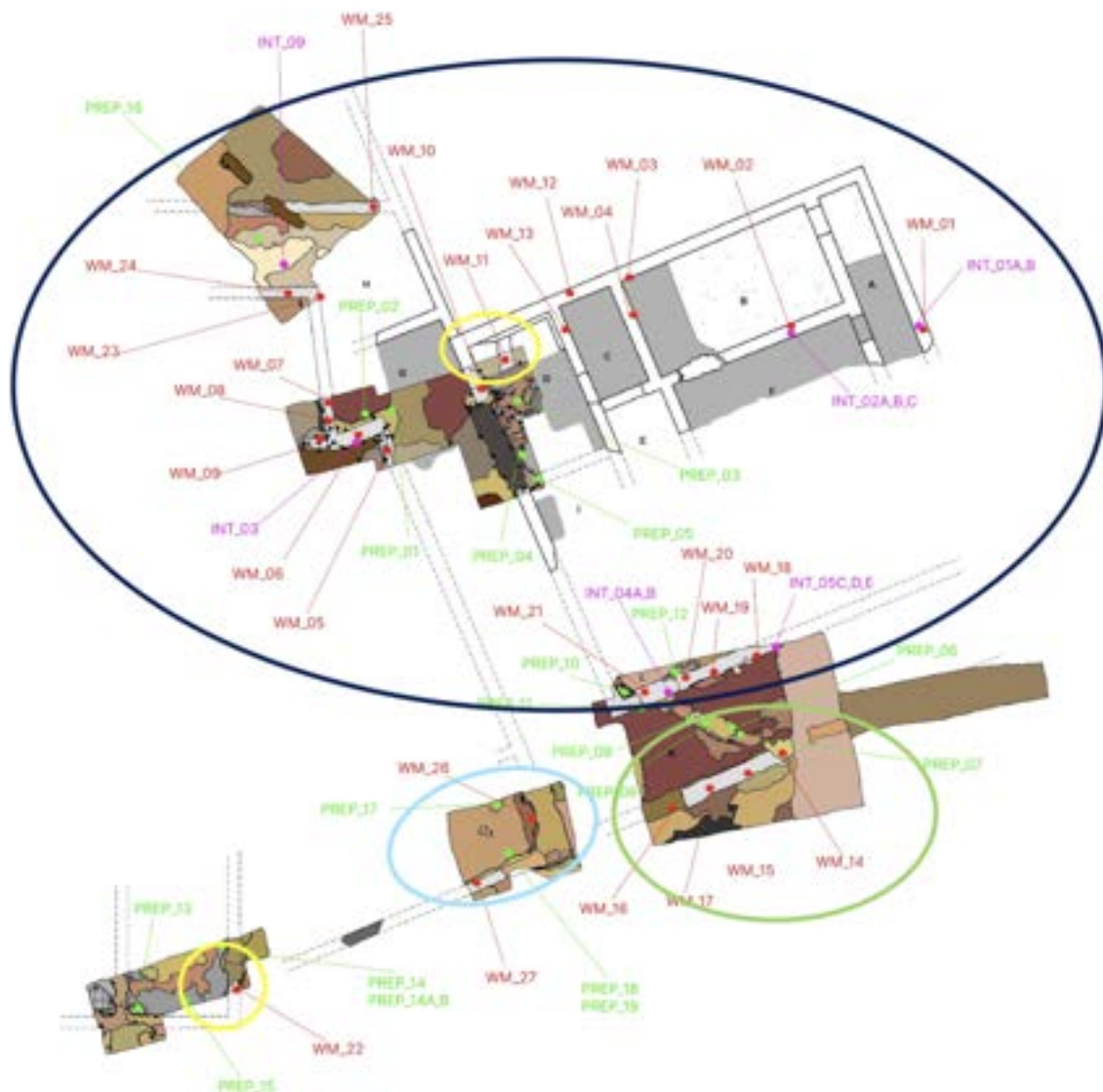

Fig. 51 Hypothesis on construction phases

Chapter 8. Conclusions

The analysis of the wall mortars of the Roman Villa of Mutteron dei Frati in Bibione enabled the identification of several construction phases based on the composition of the binders. These identified phases align closely with the earlier study conducted by Battiston and Gobbo. However, there is a minor discrepancy: according to the mortar analysis, the composition remains consistent across the phases, suggesting that only the floors underwent restoration or redecoration.

The present study reveals that the mortar composition remained consistent across all samples, with the absence of significant pozzolanic reactions indicating the use of freshwater rather than saline water in the mixing process. XRPD analysis revealed a heterogeneous aggregate composition, predominantly consisting of silicate and carbonate clasts, with minor variations between the northern and southern parts of the villa.

The aggregate grain size ranged from fine to medium sands, consistent with the local coastal dune geology, indicating local sourcing. The presence of chert and other sedimentary features suggests a history of physical weathering and transport, with both fluvial and aeolian processes contributing to the material deposition.

Three groups of mortars were classified based on their petrographic characteristics. Group 1 consists of mortars with similar characteristics, suggesting an older, consistent construction phase, with no significant compositional differences and a lack of reused mortar particles. Group 2 is defined by leaner mortars with a higher aggregate content, indicating a different or later construction phase, possibly related to the closure of an open porch. Group 3 is characterized by the presence of reused mortar pieces and a slightly higher dolomite content, suggesting a later construction phase or restoration during the Late Antiquity period.

Two notable outliers were identified. Sample WM_11, located in a lower stratigraphic layer, contains a calcination relict and is likely from an older structure. Sample WM_22, distinguished by a leaner mortar composition and higher porosity, also likely belongs to an earlier construction phase. Its wall orientation and position further support this hypothesis.

The villa likely underwent three distinct construction phases followed by a restoration period. The stratigraphic analysis supports this phased development, with the earliest phase marked by yellow, the main phase in dark blue, the enclosure of the porch in green, and wall restorations in light blue (as illustrated in Figure 51). Additionally, the preparatory layers confirm the construction phase differentiation, with Group 1 lacking cocciopesto, while samples PREP_07 and PREP_09, located in the southeastern part of the villa, include cocciopesto, indicating different construction techniques and possibly later restoration efforts.

These findings underscore the complex construction history of the Roman Villa of Mutteron dei Frati, reflecting multiple phases of building, material sourcing, and related construction techniques.

Bibliography:

1. Crisci, G.M., et al., Per. Mineral. (2004), 73, 259-268, SPECIAL ISSUE 3: A showcase of the Italian research in applied petrology
2. Kingery, W.D., Vandiver, P.B, Prickett, M., The Beginnings of Pyrotechnology, Part II: Production and Use of Lime and Gypsum Plaster in the Pre-Pottery Neolithic Near East, 1988
3. Kudlacz, K., "Phase Transitions Within the Lime Cycle: Implications in Heritage Conservation" Thesis. April, 2013. University of Granada
4. Battiston, A., Gobbo, V., Da Bibione a Baseleghe contributi per un'analisi storica del territorio, 1992, 11, 945.39, https://opac.inbiblio.it/?ids=98084
5. De Franceschini, M., Le ville romane della X regio: Venetia et Histria, 1998, ISBN 8882650197, 9788882650193
6. Gobbo, V. Concordia Sagittaria: Tremila anni di storia. Edited by P. Croce Da Villa and E. Di Filippo Balestrazzi. 2001. ISBN: 88-86413-54-8.
7. Bertolini, D., Notizie degli scavi di antichità comunicate alla R. Accademia dei Lincei per ordine di S. E. il Ministro della Pubblica Istruzione, indice topografico per l'anno 1893, Rome, Coi tipi del Salvucci, 1884
8. Busana, M.S., Architetture rurali nella Venetia romana, 2002.- XXI, 427p. :ill., ISBN 88-8265-138-X, p. 338-341
9. Comune di San Michele al Tagliamento "Dichiarazione Ambientale del Polo Turistico di Bibione" DA_PTB Rev.0 – Anno 2005
10. Arnaud-Fassetta et al., The site of Aquileia (northeastern Italy): example of fluvial geoarchaeology in a Mediterranean deltaic plain Géomorphologie : relief, processus, environnement. Octobre-décembre, vol. 9, n°4. pp. 227-245.
11. Gazzi et al., Provenienza e dispersione litoranea delle sabbie delle spiagge Adriatiche fra le Foci dell'Isonzo e del Foglia: inquadramento regionale, Mem.Soc.Geol.It., 12 (1973), 1-37, 7ff., 8 tab.
12. Venturini, C., Quattro passi nella geologia del Friuli Venezia Giulia, 2014, Università di Bologna Dipartimento di Scienze Biologiche, Geologiche e Ambientali, p.36-37
13. Ermrich, M., Opper, D., XRD for the analyst. Getting acquainted with the principles, 2013, ISBN 978-90-809086-0-4
14. Saraugi, S.S., X-Ray Diffraction (XRD)-Basic principle, instrumentation, sample preparation, XRD plots, applications of XRD, XRD sample based errors, 2024, DOI:10.13140/RG.2.2.27075.82726, Conference: Seminar and Technical Writing (FP-7998)
15. Gilchrist, A., Nobbs, J.H., Colorimetry, Theory, 2000, Encyclopedia of Spectroscopy and Spectrometry, Academic Press; ISBN-10: 0122266803
16. Shrestha, Y.K., Shrestha, S.K, Fundamentals of Colorimetry, 2023, DOI: 10.5772/intechopen.112344
17. Owsiak, Z., Microscopic methods for analysis of mortars from historical masonry structures, Bulletin of the Polish Academy of Sciences, Technical Sciences, Vol. 69(1), 2021, Article number: e136042, DOI: 10.24425/bpasts.2021.136042

18. Kirkbride, K.P., Encyclopedia of Forensic Sciences, 2000

19. Elsen et al., Hydraulicity in Historic Lime Mortars: a Review, 2nd Historic Mortars Conference HMC2010 and RILEM TC 203-RHM Final Workshop, 2010

20. Pecchioni, E., Fratini, F., Cantisani, E., Atlas of the Ancient Mortars in thin section under optical microscope, 2014, 1st edition, Isbn: 9788840443669

21. Schneider, C., Rasband, W.S., Eliceiri, K.W., NIH Image to ImageJ: 25 years of image analysis, Nature Methods, 9, 671–675 (2012)

22. Dilaria et al., High-performing mortar-based materials from the late imperial baths of Aquileia: An outstanding example of Roman building tradition in Northern Italy, 2021, DOI: 10.1002/gea.21908

23. Wentworth, C.K., 1922,The Journal of Geology: "A Scale of Grade and Class Terms for Clastic Sediments"

24. Solomon, C.J., Breckon, T.P. (2010). Fundamentals of Digital Image Processing: A Practical Approach with Examples in Matlab. Wiley-Blackwell. doi:10.1002/9780470689776. ISBN 978-0470844731.

25. Schneider CA, Rasband WS, Eliceiri KW (2012). "NIH Image to ImageJ: 25 years of image analysis". Nat Methods. **9** (7): 671–675. doi:10.1038/nmeth.2089

26. Foley, J. D.; Van Dam, A. (1982). Fundamentals of Interactive Computer Graphics. Reading, MA: Addison-Wesley. ISBN 0201144689.

27. Nesse, W.D., Introduction to Mineralogy, 2017, ISBN 0199827389

28. Schwab, F.L., Encyclopedia of Physical Science and Technology (3rd edition), 2003

29. Oliveira, M., De Souza, J., Aerial Lime mortars: An introduction and a brief discussion, Brazilian Journal of Development, 8(2), 11692–11711. https://doi.org/10.34117/bjdv8n2-216, 2022

30. Secco et al., Technological transfers in the Mediterranean on the verge of Romanization: Insights from the waterproofing renders of Nora (Sardinia, Italy), Journal of Cultural Heritage, Volume 44, July–August 2020, Pages 63-82